BMC Medicine

RESEARCH

Open Access

The regulatory variant rs1950834 confers the risk of depressive disorder by reducing *LRFN5* expression

Di Luan[1,2†], Yifan Li[1†], Aini Zhang[1†], Qingqing Bai[1†], Te Zhao[2†], Xi Chen[3], Xinglun Dang[1], Junyang Wang[4], Shaolei Jiang[5], Yun Sun[1], Yingjie Zhu[6], Yan Kong[7*], Xiong-Jian Luo[1*] and Zhijun Zhang[1,2*]

Abstract

Background Genome-wide association studies have identified 14q21.1 as a robust risk locus for major depressive disorder (MDD). However, the underlying mechanism remains elusive. Here, we aim to explore the regulatory function of rs1950834 on leucine-rich repeat and fibronectin type III domain containing 5 (*LRFN5*) expression in MDD.

Methods Clustered regularly interspaced short palindromic repeats (CRISPR)/CRISPR-associated protein 9 (Cas9)-mediated genome knockout and single-base editing were used to determine the effects of rs1950834 on the binding of transcriptional factors and the expression of the target gene *LRFN5*. Meta-analysis of multiple transcriptomic datasets was performed to clarify the brain region responsible for *LRFN5* downregulation in MDD patients. Adeno-associated virus (AAV)-mediated *Lrfn5* overexpression or knockdown in the nucleus accumbens (NAc) was used to test their effects on depression-like behaviors and sensitivity to chronic unpredictable mild stress (CUMS) in male mice. Synaptic structure and functions were monitored by synaptic protein expression assay, Golgi staining, and electrophysiological analysis.

Results The risk allele (A) of rs1950834 reduced the binding affinity to RNA polymerase II subunit A (POLR2A) and the transcription factor RAD21 cohesin complex component (RAD21), leading to decreased expression of *LRFN5*. *LRFN5* expression was downregulated specifically in the NAc of MDD patients as compared to healthy controls. Knockdown of *Lrfn5* in NAc neurons induced depression-like behaviors and further exacerbated CUMS-induced phenotypes via synaptic damage, but overexpression of *Lrfn5* in mouse NAc induced resilience to CUMS.

Conclusions These findings reveal that the functional risk single nucleotide polymorphism rs1950834 at 14q21.1 regulates *LRNN5* expression and function in NAc, providing a novel perspective for molecular diagnosis and targeted interventions of MDD.

Keywords Major depressive disorder, rs1950834, RAD21, POLR2A, LRNF5, Nucleus accumbens

†Di Luan, Yifan Li, Aini Zhang, Qingqing Bai and Te Zhao contributed equally to this work.

*Correspondence:
Yan Kong
kongyancn@163.com
Xiong-Jian Luo
luoxiongjian@seu.edu.cn
Zhijun Zhang
janemengzhang@vip.163.com
Full list of author information is available at the end of the article

Graphical Abstract

The risk allele (A) of rs1950834 reduced the binding affinity to transcription factors POLR2A and the RAD21, leading to decreased expression of *LRFN5*. *LRFN5* expression was downregulated specifically in the NAc of MDD patients and depression-like mice. Knockdown of *Lrfn5* in NAc neurons induced depression-like behaviors and further exacerbated CUMS-induced phenotypes via synaptic damage, but overexpression of *Lrfn5* in mouse NAc induces resilience to CUMS. These findings reveal that the functional risk single nucleotide polymorphism rs1950834 at 14q21.1 regulates *LRFN5* expression and function in NAc, providing a novel perspective for molecular diagnosis and targeted interventions of MDD.

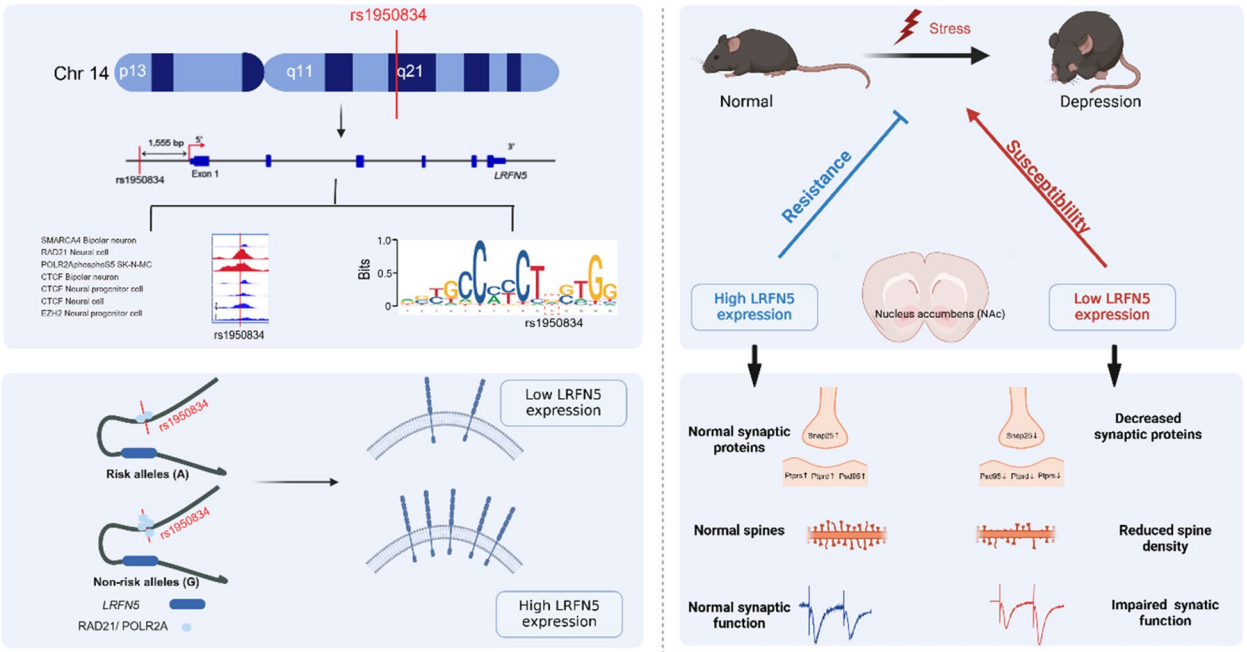

Background

Major depressive disorder (MDD) represents a debilitating mental illness with a heritability of 37% [1]. Numerous genome-wide association studies (GWASs) have identified multiple variants associated with MDD [2–6]. Unfortunately, the MDD causative genes are still elusive, leading to the lack of diagnostic markers and therapeutic targets in clinical practice. Genetic variants in linkage disequilibrium (LD) of MDD risk loci often show similar *P* values, impeding the identification of risk variants, and approximately 90% of the risk loci are located in non-coding regions. Furthermore, the function of risk variants may be brain region and cell-type specific, rendering it difficult to infer the underlying mechanisms [7]. Identification of risk variants from MDD risk loci followed by functional validation is an imperative requirement.

The rs1950834 variant of 14q21.1, located in the promoter region of leucine-rich repeat and fibronectin type III domain containing 5 (*LRFN5*), is significantly associated with depression risk [8, 9]. In addition, this variant also showed suggestive associations with cognitive function or brain structures (Additional file 1: Table S1–S3). Our previous functional genomics study preliminarily suggested that rs1950834 might be a promising functional risk variant among the 34 MDD risk SNPs disrupting the binding of 15 transcription factors (TFs) [10]. There are two alleles of rs1950834, and our previous study showed that the G allele conferred higher luciferase activities than the A allele in cell lines [10]. Further, it was predicted that the rs1950834-A was a risk allele exacerbating depression, while the rs1950834-G allele played a protective role [11]. In addition, based on the data from the 1000 Genomes Project Phase 3 [12], the frequency of the A allele varies from 48 to 80% in world populations (Additional file 1: Fig. S1). Numerous studies have consistently demonstrated that *LRFN5* may be involved in MDD pathogenesis [9, 13–15]. *LRFN5*, also known as synaptic adhesion-like molecule 5 (*SALM5*), is

a type I transmembrane protein mainly expressed in the nervous system and affects synaptic development and function [16–20]. However, it is still elusive for the regulation and function of *LRFN5* in depression. Determining whether *LRFN5* selectively modulates the function of specific neuronal subtypes in emotion-related brain regions represents a strategic approach for targeted neuromodulation in MDD.

Methods

Functional genomics analysis

To determine whether rs1950834 was located in the transcriptionally active region of the chromatin, the H3k4me3, H3k4me1, and H3k27ac chromatin immunoprecipitation-sequencing (ChIP-seq) data at the position of rs1950834 in the human brain were downloaded from Epigenome Roadmap [21], DNase I hypersensitive sites sequencing (DNase-seq) and ChIP-seq for transcription factors at the position of rs1950834 in the human brain, human neurogenic cells, and human neurogenic cell lines were queried via the Encyclopedia of DNA Elements (ENCODE) [22, 23]. The position weight matrix (PWM) data obtained from ENCODE (ENCFF606TCO and ENCFF246HIM) was analyzed using the R software package "ggseqlogo" [24].

Analysis of the correlation between transcription factors RAD21 and POLR2 A, and LRFN5 expression in the GEO datasets

Two datasets, GSE172425 [25] and GSE125413 [26], were downloaded. GSE172425 (11 controls, 12 siRad21 cases) was used to analyze the effect of *Rad21* knockdown on *Lrfn5* expression in mouse cortical neurons, while GSE125413 (3 controls, 3 *Polr2a*[R749H] mutant cases) was employed to investigate the impact of *Polr2a* mutant in mouse mature neurons on *Lrfn5* expression.

Meta-analysis of LRFN5 expression from GEO datasets

Meta-analysis using GEO datasets was used to identify brain regions where *LRFN5* was differentially expressed in depressed patients. A total of 23 datasets were downloaded, namely GSE101521 [27] (dorsolateral prefrontal cortex: 30 MDD cases, 29 healthy controls), GSE102556 [28] (anterior insula: 26 MDD cases, 22 healthy controls; cingulate gyrus: 25 MDD cases, 21 healthy controls; dorsolateral prefrontal cortex: 26 MDD cases, 22 healthy controls; nucleus accumbens: 26 MDD cases, 22 healthy controls; orbitofrontal: 26 MDD cases, 22 healthy controls; subiculum: 24 MDD cases, 19 healthy controls), GSE125664 [29] (forebrain neurons derived-iPSCs: 6 MDD cases, 3 healthy controls), GSE126512 [30] (serotonergic neurons derived-iPSCs: 6 MDD cases, 3 healthy controls), GSE169459 [31] (whole blood: 3 MDD cases, 3 healthy controls), GSE193417 [32] (anterior cingulate cortex: 6 MDD cases, 6 healthy controls), GSE32280 [33] (peripheral blood leukocyte cells: 8 MDD cases, 8 healthy controls), GSE38206 [34] (peripheral blood mononuclear cells: 9 MDD cases, 9 healthy controls), GSE39653 [35] (peripheral blood mononuclear cells: 21 MDD cases, 24 healthy controls), GSE44593 [36] (amygdala: 14 MDD cases, 14 healthy controls), GSE53987 [37] (hippocampus: 17 MDD cases, 18 healthy controls; prefrontal cortex: 17 MDD cases, 19 healthy controls; striatum: 16 MDD cases, 18 healthy controls), GSE54562 [38] (anterior cingulate cortex: 10 MDD cases, 10 healthy controls), GSE54563 [39] (anterior cingulate cortex: 25 MDD cases, 25 healthy controls), GSE54564 [40] (amygdala: 21 MDD cases, 21 healthy controls), GSE54565 [41] (anterior cingulate cortex: 16 MDD cases, 16 healthy controls), GSE54566 [42] (amygdala: 14 MDD cases, 14 healthy controls), GSE54567 [43] (dorsolateral prefrontal cortex: 14 MDD cases, 14 healthy controls), GSE54568 [44] (dorsolateral prefrontal cortex: 15 MDD cases, 15 healthy controls), GSE54571 [45] (anterior cingulate cortex: 13 MDD cases, 13 healthy controls), GSE54572 [46] (anterior cingulate cortex: 12 MDD cases, 12 healthy controls), GSE76826 [47] (peripheral blood leukocyte cells: 20 MDD cases, 12 healthy controls), GSE80655 [48] (anterior cingulate gyrus: 24 MDD cases, 24 healthy controls; dorsolateral prefrontal cortex: 23 MDD cases, 24 healthy controls; nucleus accumbens: 22 MDD cases, 22 healthy controls), and GSE98793 [49] (whole blood: 128 MDD cases, 64 healthy controls). Meta-analysis was performed using Review Manager 5.4. The expression of *LRFN5* was treated as continuous data, and the standard mean difference was used to assess the combined effect sizes. Heterogeneity was quantified using the estimated $I2$ with a Cochrane Q test. The random effects model was applied when the $I2$ level was $\geq 50\%$ or $P \leq 0.10$. Otherwise, the fixed effects model was considered.

Dual luciferase reporter gene assay

To test the impact of rs1950834 on promoter activity, the DNA fragment (513 bp) containing rs1950834 was amplified with specific primers (Additional file 1: Table S4) and inserted into the pGL4-basic vector (Promega, E6661). Vectors containing the alternative allele were generated by PCR-mediated point mutation using Golden Star T6 Super PCR mix (TSINGKE, TSE101) and Dpn I (NEB, R0176S). All constructed vectors were verified by Sanger sequencing. SH-SY5Y (4×10^4/well) and U251 (2×10^4/well) cells were plated into 96-well plates and cultured for 12 h. The reporter vectors containing the cloned fragments and control pRL-TK vectors (Renilla Luciferase) (Promega, E2241) were co-transfected into cultured cells using Lipofectamine 3000 reagent (ThermoFisher,

L3000015). Forty-eight hours post-transfection, cells were harvested, and the luciferase activity was determined using Dual-Luciferase Reporter Assay System (Promega, Cat. No. E1960) and Luminoskan Ascent instrument (Thermo Scientific).

Electrophoretic mobility shift assay

Electrophoretic mobility shift assay (EMSA) was used to study the interaction between DNA sequences and proteins (including transcription factors). The nuclear proteins of SH-SY5Y cells were extracted with the nuclear protein extraction kit (Beyotime, P0028). The biotin-labeled probes (Additional file 1: Table S5) and nucleus extracts or recombinant RAD21 and Ile1231-Lys1350 POLR2A protein from the goldORF clone were then incubated to form protein-DNA complexes. EMSA was performed using the chemiluminescence EMSA kit (Beyotime, GS009) according to the manufacturer's instructions.

ChIP-quantitative polymerase chain reaction (qPCR)

ChIP assay was performed to detect whether RAD21 and POLR2A bind to the genomic sequence containing rs1950834 in SK-N-AS cells using the ChIP kit (CST, 9002). Briefly, cells were cross-linked with 1% formaldehyde solution at room temperature for 10 min. The reaction was quenched with 2 ml 10 × glycine solution for 5 min. The cells were washed twice with cold PBS and collected with 2 ml 1 × PBS (contains 200 × protease inhibitor compound, PIC). Micrococcal nuclease (0.5 μl per 4×10^6 cells) was added and incubated at 37 °C for 20 min. Agarose gel electrophoresis was used to determine the size of DNA fragments. The IgG, H3, RAD21, and POLR2A were set as four IP groups. Crosslinked chromatin fragments (10 μg) and corresponding antibodies were added to each IP reaction, incubating at 4 °C overnight on a rotor. ChIP-level protein G magnetic beads (30 μl) were added to each immunoprecipitation reaction and incubated at 4 °C for 2 h. The enriched products were obtained by separating and rinsing the magnetic beads. The binding ability of RAD21 and POLR2A was determined by real-time qPCR (Additional file 1: Table S6).

CRISPR-Cas9-mediated genome editing

To knock out the genomic sequence containing rs1950834, we designed two sgRNAs (located upstream and downstream of rs1950834, respectively) (Additional file 1: Table S7) and cloned the sgRNAs into the PX-459 vector. RT-qPCR and Western blotting were used to verify the effect of the rs1950834 knockout on *LRFN5* expression. Primer sequences were listed in Additional file 1: Table S8.

Single-base editing was performed in SK-N-AS cells using the principle of clustered regularly interspaced short palindromic repeats (CRISPR)/CRISPR-associated protein 9 (Cas9) gene editing technology. The gRNA and ssDNA sequences are given in Additional file 1:TableS9. The successfully constructed single-base replaced cells were validated by Sanger DNA sequencing. Control (rs1950834-GG) and mutated (rs1950834-AA) SK-N-AS cells were stressed with 1 μM dexamethasone (MedChemExpress, 50–02-2,) for 72 h [50]. RT-qPCR and Western blotting were used to verify the expression of *LRFN5*.

Depression-like mouse model

Four- to six-week-old male C57BL/6J mice were purchased from GemPharmatech (Nanjing, China). All animals were subjected to a 12-h light–dark cycle (light on from 7:00 to 19:00) with food and water ad libitum at 23–25 °C and 50% humidity. The control groups housed 3–4 mice per cage, while the model groups were housed individually. Chronic unpredictable mild stress (CUMS) was used to induce depressive-like behavior in mice. The mice became acclimated to the environment and were randomly grouped after excluding outliers (baseline sucrose preference score < 70% of average). According to the randomization principle, we used a random number table for the allocation of mice to CUMS and control groups. Mice in the CUMS group were exposed to various stressors, such as swimming at 4 ℃/45 ℃ for 5 min, horizontal cage shaking for 5 min, tilting the cage at 45° for 10 h, restraint for 2 h, food/water deprivation for 12 h, clipping the tail for 1 min, tail suspension for 6 min, wet pad treatment for 12 h, followed by 12 h without padding, rat bedding for 12 h, day and night reversal, and stroboscopic light treatment for 12 h.

The sucrose preference test (SPT), tail suspension test (TST), and forced swimming test (FST) were used to measure depression-like behaviors, while the open-field test (OFT) was used to assess anxiety in mice according to the protocol published in our previous study [51, 52]. The ANY-maze animal behavior analysis system (Stoelting Co.) was used for the above detection process. For all experiments, investigators were blinded to group allocation during experimentation and data analysis. The offline data analysis was performed blindly.

Virus stereotactic injection

Mice anesthetized with sevoflurane were injected with recombinant adeno-associated virus (rAAV) (1.0×10^{13} GC/ml, 0.5 μl) in bilateral NAc (AP + 1.50 mm, ML ± 0.75 mm, and DV − 4.50 mm) to knockdown or overexpress neuron-derived *Lrfn5*. The injection rate was 0.25 μl/min. After administering the injection into the NAc, the

skull wound was sealed with bone wax. The neuron-specific overexpression and knockdown efficiency of rAAVs were validated by Western blot and immunofluorescence assay. Animals were excluded after behavior tests if they showed misinjection at postmortem examination.

Golgi-cox staining

The Hito Golgi-Cox OptimStain™ Kit was used for Golgi-cox staining. Mouse brain specimens were soaked in Golgi staining solution at 26 ℃ for 14 days. Then, the tissue treatment solution containing brain specimens was protected from light at 4 ℃ for 3 days, and Golgi developer was added dropwise for 30 min after sectioning.

Electrophysiological analysis

Whole-cell recordings were performed as described previously [53, 54]. Mice were anesthetized with isoflurane and decapitated. The brain was rapidly removed and placed in an ice-cold choline-based solution containing the following (in mM): 110 choline chloride, 2.5 KCl, 0.5 $CaCl_2$, 7 $MgCl_2$, 1.3 NaH_2PO4, 1.3 Na-ascorbate, 0.6 Na-pyruvate, 25 glucose, and 25 $NaHCO_3$, saturated with 95% O_2 and 5% CO_2. Two hundred fifty to three hundred micrometers of coronal slices containing the NAc was prepared using a vibratome. Slices were transferred to a holding chamber in an incubator containing oxygenated (95% O_2 and 5% CO_2) artificial cerebrospinal fluid (ACSF) composed of the following (in mM): 125 NaCl, 2.5 KCl, 2 $CaCl_2$, 1.3 $MgCl_2$, 1.3 NaH_2PO4, 1.3 Na-ascorbate, 0.6 Na-pyruvate, 25 glucose, and 25 $NaHCO_3$ at 32 °C for at least 1 h before recording readings. After recovery, slices were transferred to the recording chamber, where they were perfused continuously with ACSF at a flow rate of 2 ml/ min, and all experiments were performed at 23–25 °C. Recordings were obtained using a Multiclamp 700B amplifier and a Digidata 1550B (Molecular Devices). Data were sampled at 10 kHz and analyzed with a pClamp10 (Molecular Devices). Patch pipettes (4–6 MΩ) were filled with a Cs-based low Cl^- internal solution containing the following (in mM): 135 $CsMeSO_3$, 10 HEPES, 1 EGTA, 3.3 QX-314, 4 Mg-ATP, 0.3 Na-GTP, 8 Na_2-phosphocreatine, 290 mOsm kg^{-1}, adjusted to pH 7.3 with CsOH. The miniature excitatory postsynaptic currents (mEPSCs) and miniature inhibitory postsynaptic currents (mIPSCs) values were recorded at − 70 mV and 0 mV, respectively. The extracellular recording solution consisted of ACSF supplemented with picrotoxin (100 μM) and tetrodotoxin (1 μM) for the mEPSC experiment; and tetrodotoxin (1 μM), AP5 (50 μM), and CNQX (20 μM) for the mIPSC experiment. ACSF was used without any supplements for recording excitatory paired-pulse ratios (PPRs). The PPRs were elicited by electrically stimulating the NAc (0.2-ms current pulses) at − 70 mV. They were calculated by dividing the second electric-evoked excitatory postsynaptic current (EPSC) by the first, with 50 ms intervals between the two stimulations.

Statistical analysis

All values were expressed as mean ± SEM. The Shapiro–Wilk normality test was utilized to assess data distribution. For normally distributed data in this study, the results of the two sets of data were subjected to the two-tailed Student's *t*-test, while the remaining multiple sets of data were analyzed using the one-way analysis of variance with Tukey's post hoc analysis. $P < 0.05$ was considered to be statistically significant. The sample sizes are similar to those reported in previous publications.

Results

Functional genomics identifies rs1950834, located in 14q21.1, as a potential functional risk variant for depression

Based on our previous findings, we first used bioinformatic analysis to predict if rs1950834 is a functional risk single nucleotide polymorphism (SNP). Firstly, we identified that rs1950834, located in the upstream promoter region of *LRFN5* (Fig. 1A and B), was substantially enriched in signals associated with active transcription in human brain tissues, including H3k4me3, H3k4me1, and H3k27ac (Fig. 1C). Moreover, DNase-seq of human brain

(See figure on next page.)

Fig. 1 Functional genomics identified rs1950834 as a potential risk variant at depression risk locus 14q21.1. **A** LocusZoom plot showed that rs1950834 was located in a genomic region with multiple SNPs showing significant associations with MDD. **B** rs1950834 was located in the upstream promoter region of *LRFN5*. **C** ChIP-seq data showed that H3k4me3, H3k4me1, and H3k27ac preferentially bound to the genomic sequence containing rs1950834 in the human brain tissue. The heights of the colored graphs reflect the ChIP-seq signal intensities, and the location of rs1950834 is highlighted with the red line. **D** DNase-seq of human brain tissue, neurogenic cells, and cell lines consistently revealed that rs1950834 was located in the chromatin open region. **E** ChIP-seq of human neurogenic cells and cell lines showed that rs1950834 binds to transcription factors RAD21 and POLR2A. **F** and **G** PWM plots of rs1950834 binding to RAD21 and POLR2A, respectively. ChIP-Seq, Chromatin immunoprecipitation and sequencing; CTCF, CCCTC-binding factor; DNase, deoxyribonuclease; EZH2, enhancer of zeste 2 polycomb repressive complex 2 subunits; LRFN5, leucine-rich repeat and fibronectin type III domain containing 5; MDD, major depressive disorder; POLR2A, RNA polymerase II subunit A; PWM, position weight matrix; RAD21, RAD21 cohesin complex component; SMARCA4, SWI/SNF related BAF chromatin remodeling complex subunit ATPase 4

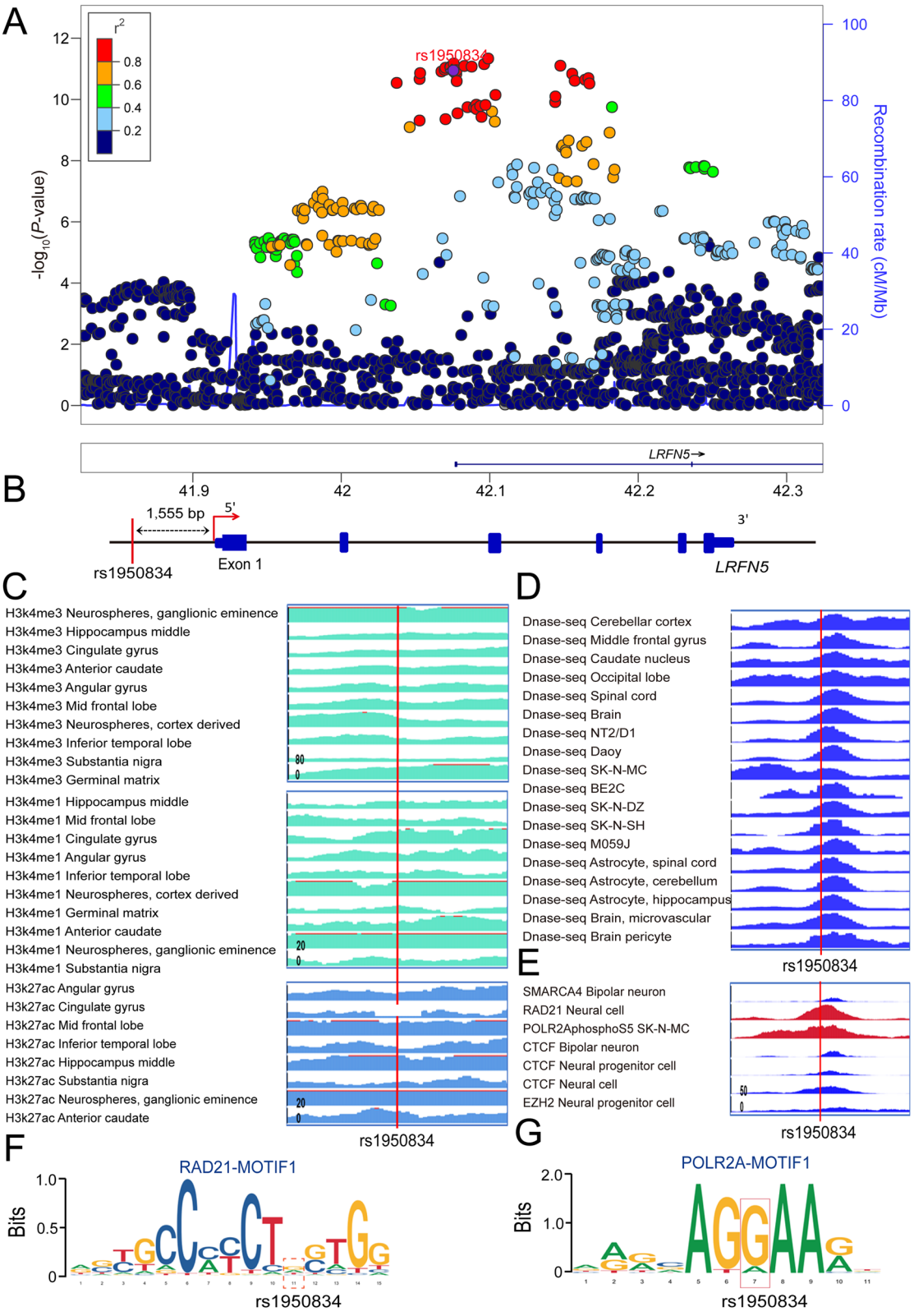

Fig. 1 (See legend on previous page.)

tissue and neurogenic cells consistently demonstrated that rs1950834 resides in an open chromatin region (Fig. 1D), supporting the fact that rs1950834 was located within a DNA region with transcription-promoting activity. Furthermore, ChIP-seq of human neurogenic cells showed that rs1950834 exhibited the strongest binding affinity to transcription factors RAD21 cohesin complex component (RAD21) and RNA polymerase II subunit A (POLR2A) (Fig. 1E). Finally, position weight matrix (PWM) analysis revealed that the A allele of rs1950834 exhibited reduced binding affinity to RAD21 (Fig. 1F) and POLR2A (Fig. 1G) compared to the G allele. These findings suggest that rs1950834 may function as a regulatory variant by modulating its binding to transcription factor RAD21 and POLR2A.

rs1950834 affects the binding of RAD21 and POLR2A which regulate the expression of *LRFN5*

To investigate the potential promoter activity of different alleles of rs1950834, we performed dual luciferase reporter gene assays, which can be used to evaluate the regulatory effect of specific DNA sequences. Inserted into the promoter region of firefly luciferase in the reporter vector, the impact of target DNA sequences on transcription can be detected by normalizing firefly luciferase activity with the control Renilla luciferase activity. The results indicated that the MDD risk rs1950834-A allele exhibited significantly reduced promoter activity compared to the rs1950834-G allele in both neuroblastoma SH-SY5Y and glioblastoma U251 cells (Fig. 2A).

Electrophoretic mobility shift assay (EMSA) is widely used to evaluate the interaction between DNA sequences and transcription factors [55, 56]. When the target DNA sequence binds a specific transcription factor, the protein-probe complexes should migrate more slowly than the corresponding free probes during electrophoresis. The EMSA results indicated that rs1950834 significantly altered binding affinities to nuclear proteins extracted from SH-SY5Y cells (Fig. 2B). The G allele of rs1950834 showed a higher affinity to transcription factors than the A allele (Fig. 2B). ChIP-seq data showed that rs1950834 loci were bound by RAD21 and POLR2A. Consistently, the EMSA results confirmed that rs1950834 affected RAD21 and POLR2A binding (Fig. 2C and D), as the band of the protein-probe complex appeared when RAD21 or POLR2A protein was added. Additionally, the binding capacity of the probe with the G allele was significantly higher than that of the A allele (Fig. 2C and D).

ChIP-qPCR and ChIP-DNA Sanger sequencing were conducted in SK-N-AS cells to test if different alleles of rs1950834 alter RAD21 and POLR2A binding affinity. ChIP-qPCR showed significant enrichment of RAD21 and POLR2A binding on the DNA region containing rs1950834 (Fig. 2E). ChIP-DNA Sanger sequencing further revealed that RAD21 and POLR2A preferred to bind the G allele than A allele at rs1950834 (Fig. 2F). These results demonstrated that different alleles of rs1950834 altered the binding affinity of RAD21 and POLR2A to the genomic sequence.

Previous studies have found a significant correlation between RAD21 or POLR2A and *LRFN5* in the human brain tissue of healthy subjects [57]. Initial analysis of the transcriptomic dataset GSE172425 [58] shows that the knockdown of *Rad21* using small interfering RNA (siRNA) resulted in decreased expression of *Lrfn5* in mouse cortical neurons (Fig. 2G). Then, after short hairpin RNA (shRNA) lentivirus targeting both *RAD21A* and *RAD21B* were constructed and delivered into SH-SY5Y and U251 cells (Fig. 2H–J), significantly decreased *LRFN5* mRNA expression (Additional file 1: Fig. S2A–D) and protein levels (Fig. 2H, K, L) as compared with the controls were observed. Similarly, another gene expression dataset (GSE125413) [59] showed that the mutation of *Polr2a* in mouse mature neurons inhibited *Lrfn5* expression (Fig. 2 M). Similarly, knockdown of the *POLR2A* by shRNA (Fig. 2N–P) led to significantly decreased *LRFN5* mRNA (Additional file 1: Fig. S2E–H) or protein (Fig. 2N, Q, R) levels in both SH-SY5Y and U251 cells. These findings underscored the regulatory role of RAD21 and POLR2A on *LRFN5* expression. Collectively, rs1950834 may influence the expression of *LRFN5* by regulating the DNA binding affinity of RAD21 and POLR2A.

rs1950834 directly regulates *LRFN5* expression

Then we further elucidated whether rs1950834 can directly regulate the expression of the target gene *LRFN5*. The cis-expression quantitative trait loci (cis-eQTL) analysis showed that only *LRFN5* expression was significantly associated with rs1950834 among all the genes located within 1 Mb upstream and downstream of rs1950834 in BrainMeta v2 and PsychENCODE (Fig. 3A and B). Therefore, the subsequent research focused on *LRFN5* as the target gene of rs1950834. Moreover, we explored whether the effects attributed to the unique rs1950834 genotype on *LRFN5* expression levels, in which an analysis of human brain eQTLs found that the levels of *LRFN5* expression were affected by gene dose efficacy (Additional file 1: Fig. S3A–D). The A allele of rs1950834 reduced *LRFN5* expression compared to the G allele in different human brain regions (Additional file 1: Fig. S3A-D). Importantly, the knockout of the DNA segment containing rs1950834 via CRISPR-Cas9 gene editing led to a decrease in both *LRFN5* mRNA expression (Fig. 3C and E) and protein level (Fig. 3D and F) in SH-SY5Y cells. Furthermore, to provide direct

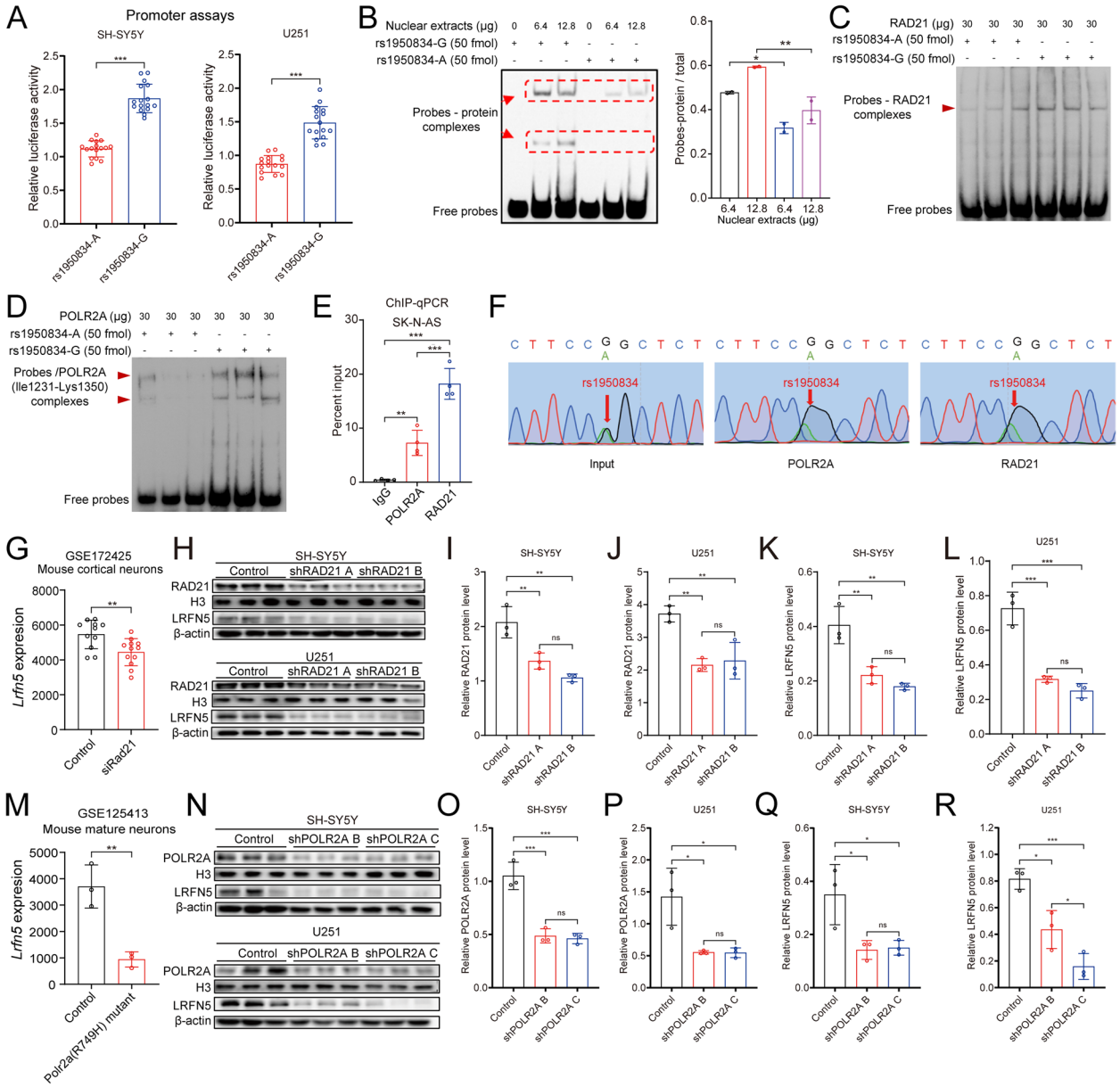

Fig. 2 rs1950834 regulated *LRFN5* expression by affecting the binding of RAD21 and POLR2A. **A** Reporter gene assays showed that different alleles of rs1950834 significantly affected luciferase activity. Compared with the A allele, the G allele of rs1950834 conferred significantly higher luciferase activity in both SH-SY5Y and U251 cells ($N = 16$ in each group). Two-tailed unpaired t-test. ***$P < 0.001$. Mean ± SEM. **B**–**D** rs1950834 affected the binding affinity of nuclear protein extracts. The quantification data (grey values, arbitrary units) of the probes/protein complexes were first quantified using Image J. The obtained values were then normalized to the total quantity of probes. **B** For rs1950834, the G allele showed stronger binding of 6.4 μg or 12.8 μg nuclear extracts than the A allele ($N = 2$ in each group). Two-tailed unpaired t-test. *$P < 0.05$. **$P < 0.01$. Mean ± SEM. **C** and **D** rs1950834 affected RAD21 and POLR2A binding affinity. Competitive experiments showed that the G allele had stronger RAD21 and POLR2A binding than the A allele. **E** Significant enrichment of RAD21 and POLR2A on genomic sequences containing rs1950834 by ChIP-qPCR. DNA templates from cross-linked chromatins of cells (with IgG immunoprecipitation) were used in the IgG group ($N = 4$ in each group). One-way ANOVA followed by Tukey's post hoc test. **$P < 0.01$, ***$P < 0.001$. Mean ± SEM. **F** ChIP-sequencing analysis on the binding ability of the A or G allele to RAD21 and POLR2A in the whole-genome context in SK-N-AS cells. **G** Analysis of the GSE172425 dataset on the expression of *Lrfn5* after knockdown of *Rad21* by siRNA in the primary cultured mouse cortical neurons ($N = 11$ in the Control group, and $N = 12$ in the siRad21 group). Two-tailed unpaired t-test. **$P < 0.01$. Mean ± SEM. **H**–**L** *LRFN5* expression was significantly decreased by shRNA lentivirus targeting both *RAD21A* and *RAD21B* in SH-SY5Y and U251 cells. The reduced expression of *RAD21* mRNA (shown in Additional file 1: Fig. S2) or protein was found both in SH-SY5Y and U251 cells, confirming the successful knockdown of *RAD21* (N = 3 in each group). One-way ANOVA followed by Tukey's post hoc test. **$P < 0.01$, ***$P < 0.001$. Mean ± SEM. **M** The GSE125413 dataset showed that *Polr2a* mutations decreased *Lrfn5* expression in mature neurons of mice ($N = 3$ in each group). Two-tailed unpaired t-test. **$P < 0.01$. Mean ± SEM. **N**–**R** *POLR2A* knockdown in SH-SY5Y and U251 cells affected *LRFN5* expression significantly ($N = 3$ in each group). One-way ANOVA followed by Tukey's post hoc test. *$P < 0.05$, ***$P < 0.001$. Mean ± SEM

evidence that rs1950834 affected *LRFN5* expression levels, we successfully utilized single-base editing technology to generate rs1950834-AA and rs1950834-GG genotypes in SK-N-AS cells (Fig. 3G). This approach directly revealed the decreased expression of *LRFN5* mRNA (Fig. 3H and I) and protein (Fig. 3J–L) in the MDD risk-associated rs1950834-AA genotype compared to the rs1950834-GG genotype in both naive and dexamethasone (DEX)-stressed conditions.

Then, utilizing the SK-N-AS cells of rs1950834-AA and rs1950834-GG genotypes, we performed RNA-seq for transcriptomic analysis to further elucidate the pathways regulated by rs1950834. In the naive state, the rs1950834-AA genotype exhibited 2087 upregulated genes and 2480 downregulated genes, resulting in a total of 4567 differentially expressed genes (DEGs) compared with the rs1950834-GG genotype (Fig. 3M) ($Log_2|FC| > 2$, $FDR < 0.05$). Under DEX stress conditions, the rs1950834-AA genotype exhibited 2800 upregulated genes and 3191 downregulated genes, resulting in a total of 5991 DEGs compared with the rs1950834-GG genotype (Fig. 3M) ($Log_2|FC| > 2$, $FDR < 0.05$). Finally, to understand shared biological processes between rs1950834 genotypes in the presence and absence of DEX stress, we selected the intersection of DEGs among AA vs GG and AA + DEX vs GG + DEX, resulting in a total of 3764 DEGs for subsequent GO and KEGG analyses (Fig. 3M). In GO-biological processes enrichment, DEGs were mainly associated with neuron projection morphogenesis, cell–cell adhesion, and axonogenesis. In GO-cellular components, it was associated with synaptic structures, while in GO-molecular functions, it was related to cell adhesion (Fig. 3N). KEGG analysis revealed enrichment in differentially expressed genes in synapses and adhesion pathways, including focal adhesion, axon guidance, and cell adhesion molecules (Fig. 3O). This provides valuable insights into elucidating the rs1950834-regulated interactions among synaptic-associated proteins of the target gene *LRFN5*.

Role of NAc neuron-derived *LRFN5* in depression

As the A allele of rs1950834 reduced promoter activity of *LRFN5* via regulating the DNA binding affinity of transcription factor RAD21 and RNA polymerase subunit POLR2A, it was necessary to investigate cell type and brain region specificity of *LRFN5* downregulation in MDD. We first performed tissue-specificity expression analysis of *LRFN5* using expression data from the GTEx (https://www.gtexportal.org/) (GTEx Consortium, 2013). *LRFN5* is expressed in many human tissues. However, *LRFN5* expression in brain tissues is relatively high compared with other tissues (Additional file 1: Fig. S4). Cell-type-specific expression analysis using the data from the Allen Brain Map (https://celltypes.brain-map.org/rnaseq/human_m1_10x) showed that *LRFN5* exhibits its predominant expression in neurons and low expression in glial cells (Additional file 1: Fig. S5).

We also examined the associations between *LRFN5* and other psychiatric disorders (including attention deficit and hyperactivity disorder, anorexia nervosa, anxiety disorder, autism spectrum disorder, bipolar disorder, and schizophrenia) using published GWAS summary statistics [60–65]. Genetic variants near *LRFN5* (within a ± 250 kb window upstream and downstream of the gene) did not show genome-wide significant associations ($P < 5 \times 10^{-8}$) with attention deficit and hyperactivity disorder (Additional file 1: Fig. S6A), anorexia nervosa (Additional file 1: Fig. S6B), anxiety disorder (Additional file 1: Fig. S6C), autism spectrum disorder (Additional file 1: Fig. S6D), bipolar disorder (Additional file 1: Fig. S6E), and schizophrenia (Additional file 1: Fig. S6F), implying that the association of *LRFN5* is specific to MDD.

Then, we performed a meta-analysis of transcription data of MDD patients from the GEO database to identify *LRFN5* differentially expressed brain regions in depressed patients (Additional file 1: Fig. S7A–H). The results demonstrated no significant differential expression of *LRFN5* in the peripheral blood, frontal cortex, amygdala, and cingulate cortex between the MDD patients and the controls. Interestingly, *LRFN5* was selectively decreased in

(See figure on next page.)

Fig. 3 rs1950834 regulated the expression of LRFN5 as validated in gene editing cells. **A** and **B** The eQTL analysis of rs1950834 and its surrounding genes within a 1 M bp window, e.g., 500 kb upstream and 500 kb downstream of rs1950834, respectively, in BrainMeta v2 and PsychENCODE eQTL dataset. Expression of *LRFN5* showed the most significant associations with rs1950834. **C** Schematic diagram and validation of rs1950834 knockout. **D**–**F** rs1950834 knockout downregulated expression of *LRFN5* mRNA and protein level in SH-SY5Y cells ($N = 3$ in each group). Two-tailed unpaired t-test. $^{**}P < 0.01$, $^{***}P < 0.001$. Mean ± SEM. **G** The successful construction of rs1950834-AA and rs1950834-GG genotypes in SK-N-AS cells. **H** and **I** *LRFN5* mRNA expression levels were lower in the rs1950834-AA genotype compared to the rs1950834-GG genotype in both naive and DEX-stressed states ($N = 3$ in each group). $^{*}P < 0.05$, $^{***}P < 0.001$. Mean ± SEM. **J** Western blot analysis showed that LRFN5 protein levels were lower in the rs1950834-AA genotype compared to the rs1950834-GG genotype in both **K** naïve and **L** DEX-stressed states, $N = 6$ in each group. $^{**}P < 0.01$, $^{***}P < 0.001$. Mean ± SEM. **M** Differentially expressed genes (DEGs) (Log2|FC > 2|, FDR < 0.05) of bulk RNA-seq in the rs1950834-AA and rs1950834-GG genotypes in naive and DEX-stressed conditions. **N** GO analysis of the differentially expressed genes. **O** KEGG analysis of the differentially expressed genes. Data were analyzed using the two-tailed unpaired t-test and are expressed as the mean ± SEM. $^{*}P < 0.05$, $^{**}P < 0.01$, $^{***}P < 0.001$

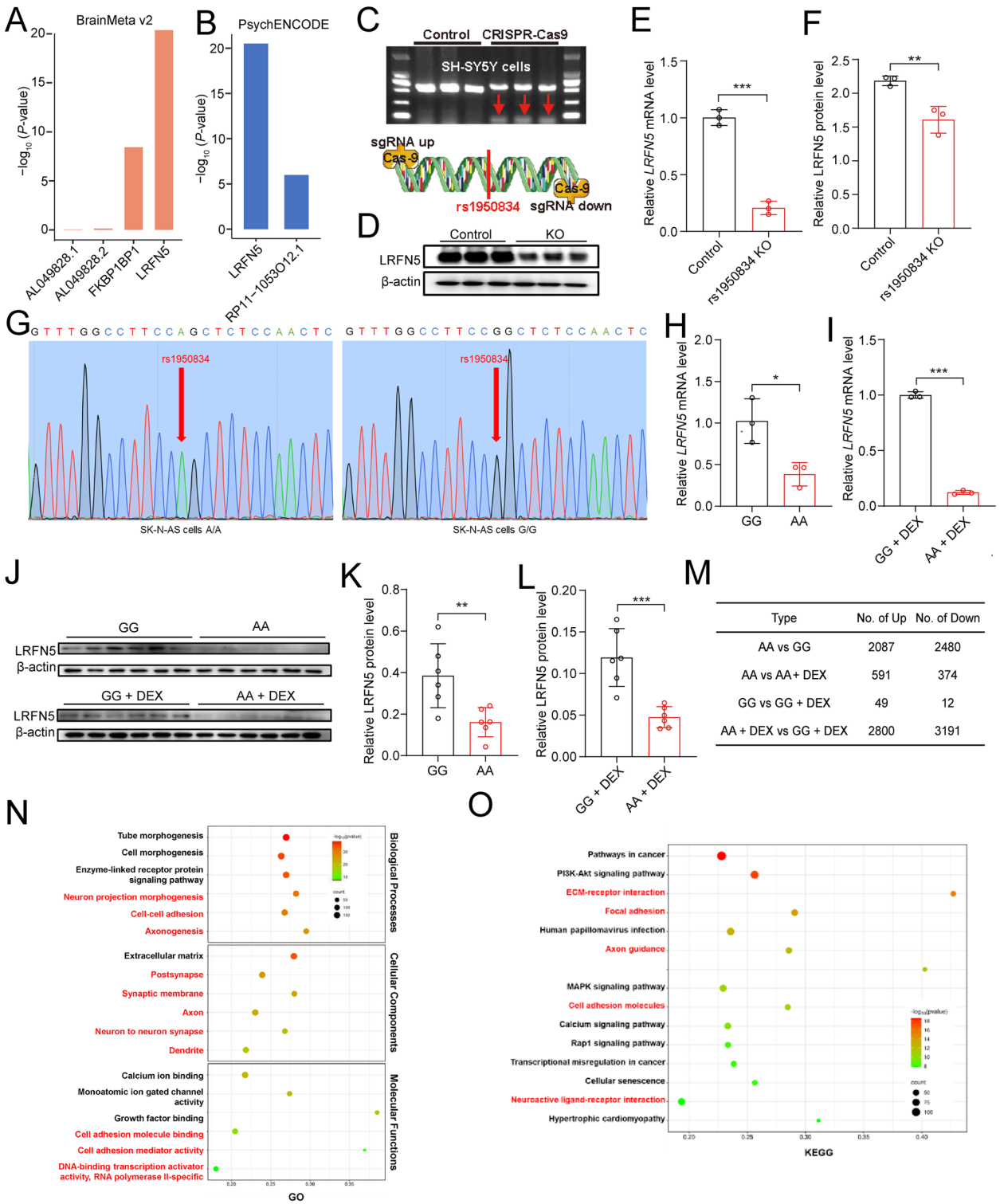

Fig. 3 (See legend on previous page.)

the NAc of MDD patients (Additional file 1: Fig. S7H). As one of the emotion-related brain regions, NAc could be important for *LRFN5* function in MDD [66].

Thereby, to validate the above results, we examined whether the differential expression of *Lrfn5* was neuronal cell subtype-specific in the NAc of CUMS-induced

depressive-like mice. As shown in Fig. 4A and B, mice with CUMS-induced depression-like phenotypes exhibited decreased sucrose preference and increased immobile time in the TST and FST compared to wildtype mice. Importantly, a significant reduction in LRFN5 protein expression in $NeuN^+$ neurons was found in the NAc of depressed mice (Fig. 4C), but not those of $GFAP^+$ astrocytes (Fig. 4D) and $Iba1^+$ microglia (Fig. 4E). The expression of *LRFN5* in neurons was negatively correlated with depression-like phenotypes in SPT and FST (Fig. 4F), suggesting that NAc neuron-derived LRFN5 played critical roles in depression pathogenesis.

The NAc consists of three subregions, namely the nucleus, the medial shell, and the lateral shell, and 95% of the NAc is composed of medium spiny neurons (MSNs) with dopamine receptor D1 (DRD1) and dopamine receptor D2 (DRD2) markers, respectively. Subsequently, we explored whether *LRFN5* dysregulation specifically occurred in functional subregions and neuronal subtypes. The results showed that *LRFN5* was broadly downregulated in $DRD1^+$ and $DRD2^+$ MSNs in the NAc core, and the medial and lateral shell of CUMS-stressed mice compared to controls (as shown in Fig. 4G–J). Taking together, in CUMS-induced depressive-like mice, neuron-derived LRFN5 protein were ubiquitously reduced in NAc, with no subregion or neuronal cell type specificity.

NAc neuron-derived *LRFN5* plays an important role in depression by affecting synapse-related functions

To further validate whether the NAc neuron-derived *LRFN5* was involved in the occurrence of depression, we constructed *Lrfn5* overexpression or knockdown mouse models via rAAV-injection into NAc (Fig. 5A and Additional file 1: Fig. S8). Western blot analysis showed significantly reduced LRFN5 protein levels in the knockdown mice, while significantly increased LRFN5 protein levels were in the overexpression mice as compared to rAAV controls (Fig. 5B), confirming the successful construction of *Lrfn5* gain-of-function and loss-of-function models. Compared with the rAAV control group, the rAAV knockdown mice exhibited depression-like behavior indicated by decreased sucrose preference and increased immobility time for forced swimming (Fig. 5C). Furthermore, *Lrfn5* knockdown exacerbated the CUMS-induced depressive phenotypes of the mice (Fig. 5D–F), while the *Lrfn5* overexpressing mice exhibited increased resistance to CUMS (Fig. 5D–F), suggesting that NAc neuron-derived *LRFN5* plays a critical protective role in depression and may serve as a potential therapeutic target.

As *LRFN5* affects synaptic development and function [17, 18] through adhesion molecules [19], we first examined the role of *LRFN5* on synaptic functions in the NAs. Compared with the rAAV control group, the CUMS rAAV group showed markedly decreased expression of synapse-associated proteins, including protein tyrosine phosphatase receptor type D (PTPRD), postsynaptic density protein 95 (PSD95), and synaptosome-associated protein 25 (SNAP25) (Fig. 6A), along with a reduced total dendritic spine density (Fig. 6C), the density (Fig. 6E) and the proportion of stubby spines (Fig. 6F) in the NAc. As the changes in spine structure indicate synaptic activity, the dysregulation of spine morphology, especially for the mature thin, stubby, and mushroom subtypes, underlies CUMS-induced depression-like behaviors and serves as a target for combined magnetic stimulation system treatment [51, 52]. Interestingly, stubby spines lack a clear distinction between head and neck, which allows the diffusion of elevated calcium transients at the synapse into the dendritic shaft [67]. These observations were further aggravated in the CUMS + shLrfn5 group (Fig. 6C–F). In contrast, the *Lrfn5* overexpression in NAc neurons significantly reversed the CUMS-induced synaptic abnormities (Fig. 6C–F).

(See figure on next page.)

Fig. 4 NAc neuron-derived *Lrfn5* was involved in depression. **A** Flow chart of the animal experiment for CUMS-induced depressive-like behavior. **B** Compared with the controls, the CUMS group showed decreased sucrose preference ($P < 0.01$), increased immobility time of the tail suspension test ($P < 0.01$), and forced swimming test ($P < 0.05$), $N = 7$ in the Control and CUMS group. **C**–**E** Immunofluorescence of LRFN5 with NeuN, GFAP, and Iba1 in mouse NAc. Compared with the control group, the number of $NeuN^+LRFN5^+$ cells in the CUMS group were decreased ($P < 0.01$), while $GFAP^+LRFN5^+$ ($P > 0.5$) and $Iba1^+LRFN5^+$ ($P > 0.5$) had no significant difference in NAc of mice ($N = 3$ in each group). **F** The number of $NeuN^+LRFN5^+$ cells was correlated to the scores of SPT and FST ($N = 6$ in each group). **G**–**J** Immunofluorescence of LRFN5 in the DRD1 or DRD2 MSNs in three subregions of NAc, including core, medial, and lateral shell, respectively (**G** and **H**). The results showed that $DRD1^+LRFN5^+$ and $DRD2^+LRFN5^+$ MSNs were generally downregulated in the NAc core, media, and lateral shell of CUMS-stressed mice compared to controls without the differences in subregion and neuronal subtype specificity (**I** and **J**), $N = 6$ in each group. DAPI, 4′,6-diamidino-2-phenylindole; DRD1, dopamine receptor D1; DRD2, dopamine receptor D2; MSN, medium spiny neuron; FST, forced swimming test; GFAP, glial fibrillary acidic protein; Iba1, ionized calcium-binding adaptor molecule 1; IF, immunofluorescence; L, lateral; LRFN5, leucine-rich repeat and fibronectin type III domain containing 5; M, medial; NAc, nucleus accumbens; NeuN, neuronal nuclei antigen; WB, Western blot. Data were analyzed using the two-tailed unpaired *t*-test and are expressed as the mean ± SEM. $^*P < 0.05$, $^{**}P < 0.01$, $^{***}P < 0.001$

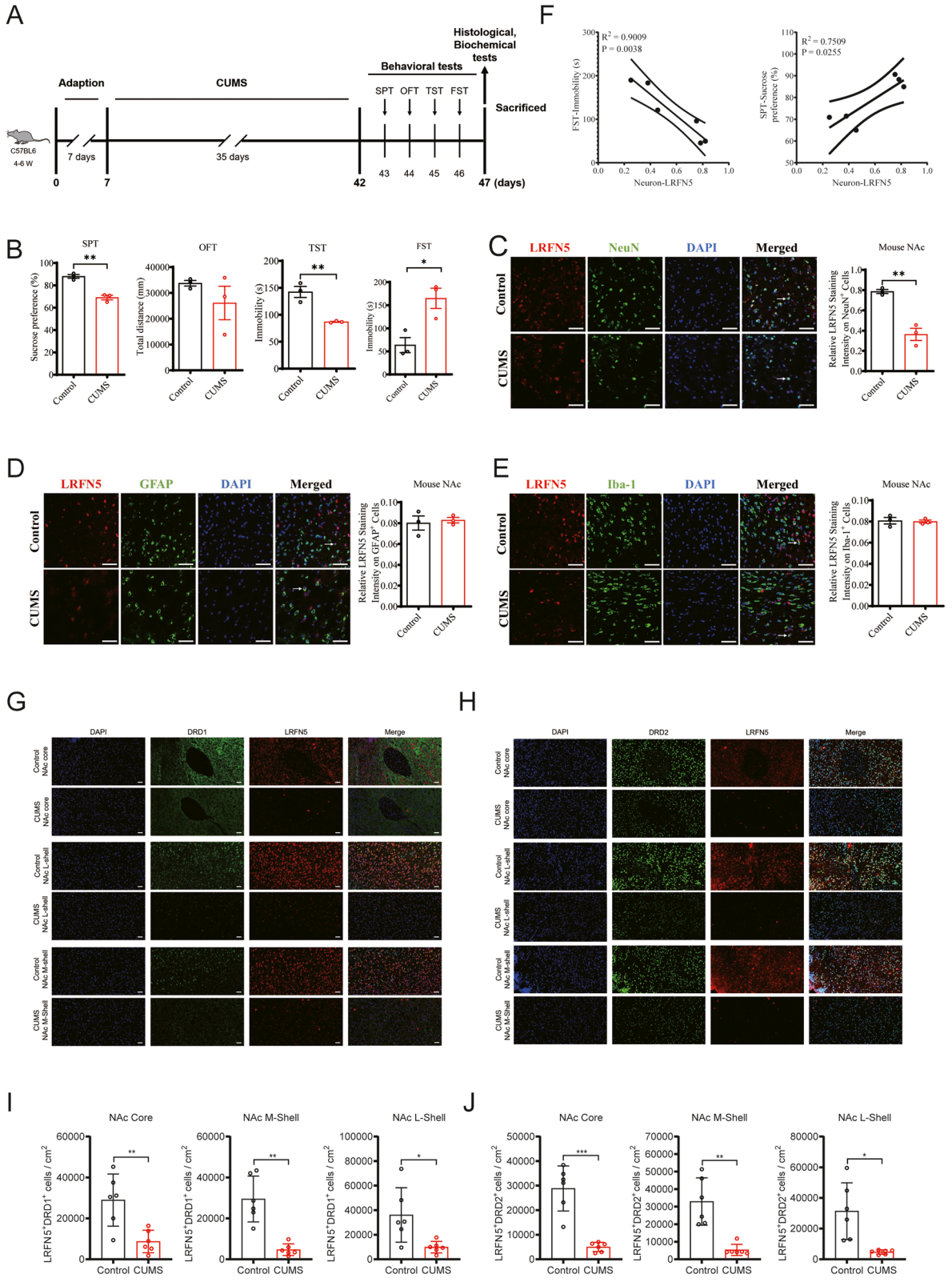

Fig. 4 (See legend on previous page.)

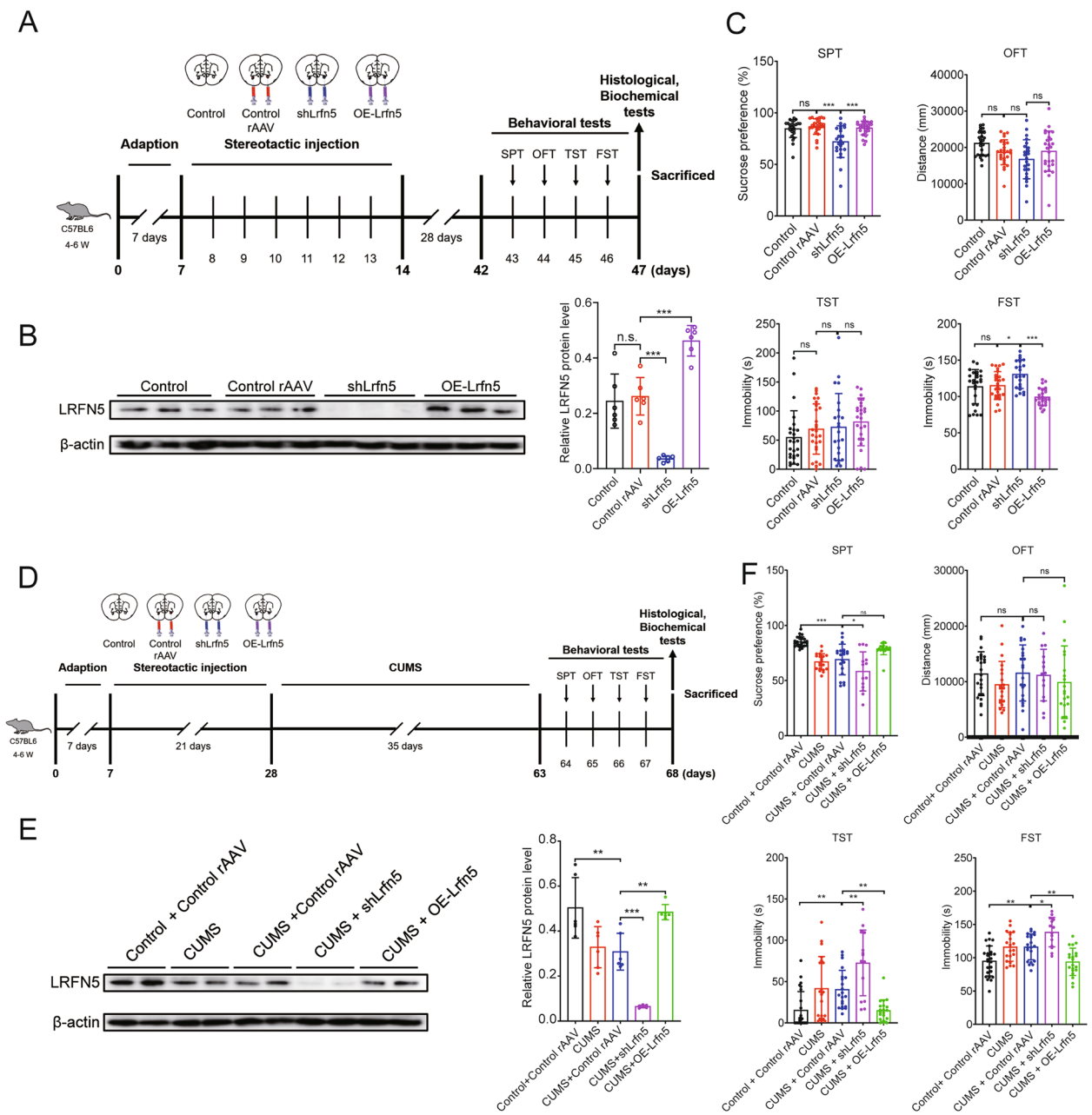

Fig. 5 NAc neuron-derived *Lrfn5* participates in the occurrence of depression. **A** Flow chart of the animal experiment for knockdown or overexpression of neuron-derived *Lrfn5* in NAc on CUMS-induced depressive-like behaviors. **B** Western blotting measures LRFN5 protein levels among control, control rAVV, shLrfn5, and OE-Lrfn5 group mice to verify successful construction ($N=6$ in each group). One-way ANOVA followed by post hoc Tukey's test, $^{*}P<0.05$, $^{**}P<0.01$, $^{***}P<0.001$, ns, no significant difference. Each bar represents the mean ± SEM. **C** The downregulation of NAc neuron-derived *Lrfn5* expression induced depressive-like behaviors, while the upregulation of NAc neuron-derived *Lrfn5*had no effects ($N=26$ in Control group, $N=27$ in Control rAAV group, $N=23$ in shLrfn5 group, $N=26$ in OE-Lrfn5 group). One-way ANOVA followed by post hoc Tukey's test, $^{*}P<0.05$, $^{**}P<0.01$, $^{***}P<0.001$, ns, no significant difference. Each bar represents the mean ± SEM. **D** Flow chart of the animal experiment for CUMS-induced depressive-like behavior in knockdown or overexpression of neuron-derived *Lrfn5* in NAc mice. **E** Western blotting of LRFN5 levels among each group of mice ($N=6$ in each group). One-way ANOVA followed by post hoc Tukey's test, $^{*}P<0.05$, $^{**}P<0.01$, $^{***}P<0.001$, ns, no significant difference. Each bar represents the mean ± SEM. **F** Knockdown of NAc neuron-derived *Lrfn5* of mice increased susceptibility to CUMS-induced depressive-like behaviors, while overexpression of NAc neuron-derived *Lrfn5* of mice increased resistance to the above phenotype ($N=25$ in Control + Control rAAV group, $N=20$ in CUMS group, $N=21$ in CUMS + Control rAAV group, $N=11$ in CUMS + shLrfn5 group, $N=20$ in CUMS + OE-Lrfn5 group). One-way ANOVA followed by post hoc Tukey's test, $^{*}P<0.05$, $^{**}P<0.01$, $^{***}P<0.001$, ns, no significant difference. Each bar represents the mean ± SEM. KD, knockdown; OE, overexpression

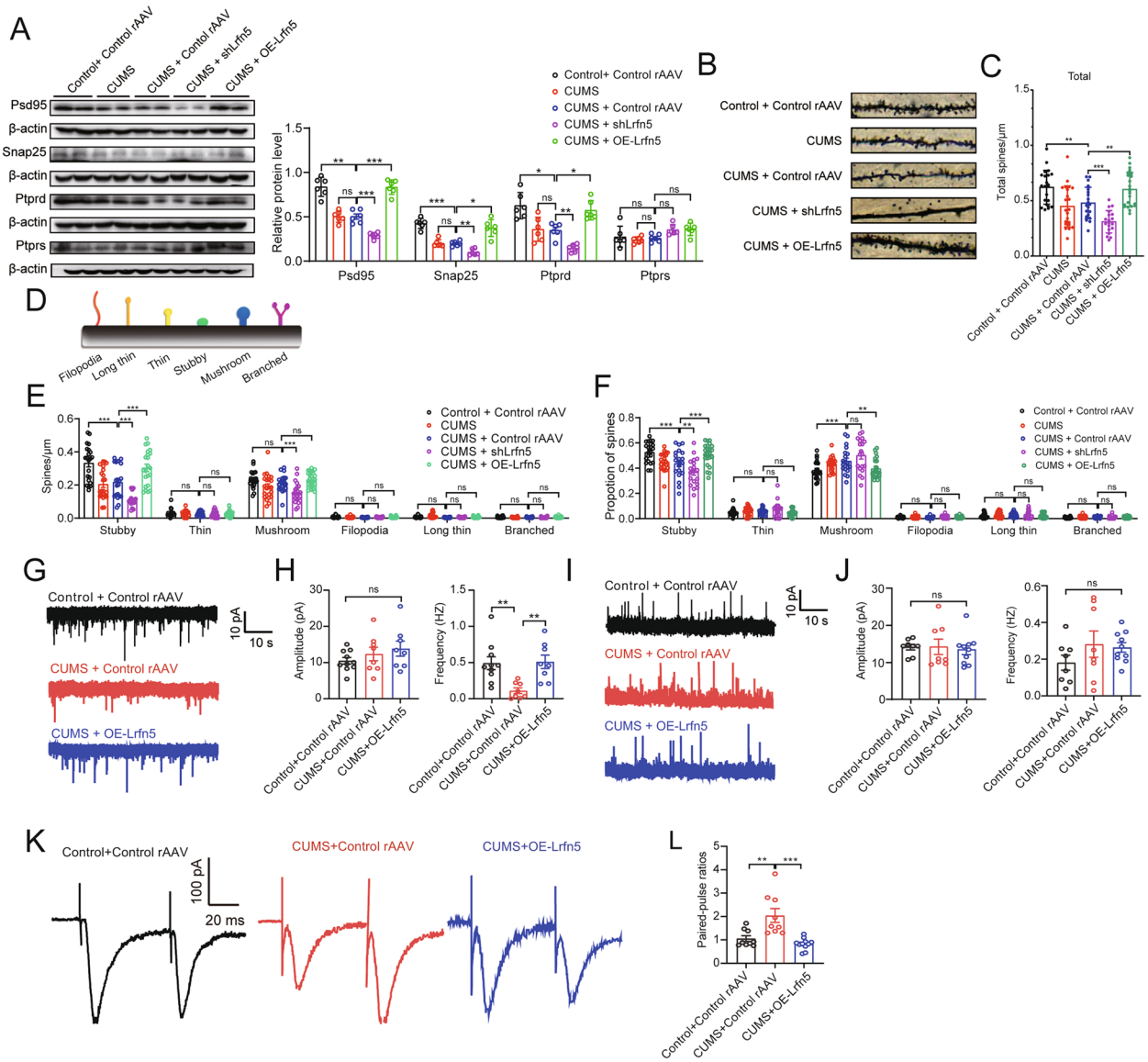

Fig. 6 Synaptic structure and function influenced by NAc neuron-derived *Lrfn5* in depression. **A** Western blotting with quantification of synaptic protein levels in the NAc in Control + Control rAAV, CUMS (non-rAAV injected), CUMS + Control rAAV, CUMS + sh-Lrfn5, andCUMS + OE-Lrfn5 ($N = 6$ in each group). Two-way ANOVA followed by Tukey's post hoc test, $^{*}P < 0.05$, $^{**}P < 0.01$, $^{***}P < 0.001$. **B**–**F** Golgi-Cox stained dendritic spines and spine density quantification in the NAc in Control + Control rAAV, CUMS (non-rAAV injected), CUMS + Control rAAV, CUMS + sh-Lrfn5, and CUMS + OE-Lrfn5 ($N = 22$ in Control group, $N = 22$ in CUMS group, $N = 20$ in CUMS + Control rAAV group, $N = 19$ in CUMS + shLrfn5 group, $N = 23$ in CUMS + OE-Lrfn5 group). **D** The schematic diagram of different types of spines. Filopodia spines are > 2 μm in length; the maximum width of stubby spines is less than their length; long thin spines are 1–2 μm in length; thin spines are < 1 μm in length; mushroom spines have a head/neck diameter ratio > 1; branched spines have more than one spine head attached to same spine neck. **C** One-way ANOVA followed by post hoc Tukey's test, $^{*}P < 0.05$, $^{**}P < 0.01$, $^{***}P < 0.001$, ns, no significant difference. **E** and **F** Two-way ANOVA followed by Tukey's post hoc test. **G** Representative traces of mEPSCs from the Control group (black), CUMS group (red), and OE-Lrfn5 + CUMS group (blue). **H** Left: Average amplitudes of mEPSCs for the Control group ($N = 10$), CUMS group ($N = 8$), and CUMS + OE-Lrfn5 group ($N = 8$). One-way ANOVA followed by post hoc Tukey's test, ns, no significant difference. Right: Average frequencies of mEPSCs for the Control group ($N = 10$), CUMS group ($N = 8$), and CUMS + OE-Lrfn5 group ($N = 8$). One-way ANOVA followed by post hoc Tukey's test, $^{**}P < 0.01$. Each bar represents the mean ± SEM. **I** Representative traces of mIPSCs from the Control group (blank), CUMS group (red), and OE-Lrfn5 + CUMS group (blue). **J** Left: Average amplitudes of mIPSCs for the Control group ($N = 8$), CUMS group ($N = 8$), and OE-CUMS + Lrfn5 group ($N = 10$). One-way ANOVA followed by post hoc Tukey's test, ns, no significant difference. Right: Average frequencies of mIPSCs for the Control group ($N = 8$), CUMS group ($N = 8$), and CUMS + OE-Lrfn5 group ($N = 10$). One-way ANOVA followed by post hoc Tukey's test, ns, no significant difference. Each bar represents the mean ± SEM. **K** and **L**, Example traces (**K**) and quantification (**L**) of the paired-pulse ratio of electrical stimulation-evoked EPSCs in NAc neurons ($N = 9$ in Control group, $N = 9$ in CUMS group, $N = 11$ in CUMS + OE-Lrfn5 group). One-way ANOVA followed by post hoc Tukey's test, $^{**}P < 0.01$, $^{***}P < 0.001$. Each bar represents the mean ± SEM. mEPSC, miniature excitatory postsynaptic current; mIPSC, miniature inhibitory postsynaptic current

To investigate the impact of *Lrfn5* overexpression on CUMS-impaired synaptic transmission of median-spiny neurons, whole-cell patch clamp recordings were performed on acute NAc brain slices. We observed a significant reduction in the frequency, but not amplitude, of miniature excitatory postsynaptic currents (mEPSCs) in CUMS rAAV mice (Fig. 6G and H), indicating a decrease in α-amino-3-hydroxy-5-methyl-4-isoxazole propionic acid (AMPA) receptor-mediated excitatory synaptic transmission. This reduction in mEPSC frequency was ameliorated by *Lrfn5* overexpression (Fig. 6G and H). We did not observe a significant difference in the frequency and amplitude of miniature inhibitory postsynaptic currents (mIPSCs) between the control rAAV group, CUMS rAAV group, and *Lrfn5* overexpressing mice (CUMS + OE-Lrfn5 mice) (Fig. 6I and J). Next, we examined presynaptic function by measuring the paired-pulse ratio (PPR). The PPR was significantly increased in the CUMS rAAV mice, indicating a reduction of presynaptic release probability. This increase in PPR was reversed by *Lrfn5* overexpression (Fig. 6K and L). These results suggest that impaired synaptic transmission in the NAc of CUMS mice could be rescued by *Lrfn5* overexpression.

These findings suggested that NAc neuron-derived LRFN5 is a key molecule involved in depression through the maintenance of synaptic function and might serve as a potential molecular target for MDD interventions.

Discussion

Our findings have demonstrated for the first time that the MDD risk-associated rs1950834 allele A decreased the binding of transcription factor RAD21 and RNA polymerase subunit POLR2A, leading to reduced promoter activity and expression of the target gene *LRFN5*. This study revealed that *LRFN5* expression was significantly reduced in the NAc of MDD patients. Knockdown of NAc neuron-derived *Lrfn5* induced depression-like behavior and further exacerbated the phenotype caused by CUMS in mice, while *Lrfn5* overexpression induced resistance to CUMS. Furthermore, the study illustrated the potential mechanism of decreased NAc neuron-derived LRFN5 protein in depression via synaptic dysfunction. These findings offered new insights and evidence for the diagnosis, molecular targeted intervention, and precise neuromodulation of MDD.

This study comprehensively used bioinformatic tools, knockout or knock-in cell lines, and the depression-like mouse model. We successfully constructed SK-N-AS cells with rs1950834 AA and GG genotypes by CRISPR-Cas9-mediated single-base editing for the first time, which verified the bioinformatics findings that the role of rs1950834 is in regulating the target gene expression. Transcriptomic datasets were used to identify NAc as the key emotional brain region responsible for the dysregulation of *LRFN5* in depression, which were further validated for the contribution to depression by rAAV-mediated gene overexpression or knockdown. Subregional and neuron subtype specificity for *Lrfn5* downregulation was precisely characterized in CUMS-induced depression-like mice. The contribution of *Lrfn5* to neuron structure and function was systematically validated by measuring synaptic proteins, Golgi staining, and electrophysiological analysis. Collectively, the utilization of state-of-the-art methodologies improves the reliability of experimental results.

The most important contribution of this study is that it provides systematic and direct evidence that MDD risk-associated allele A of rs1950834 exhibited reduced binding affinity with RAD21 and POLR2A, leading to reduced promoter activity and expression of *LRFN5*. The interpretation of abundant risk loci for MDD identified by GWAS has become crucial in the post-GWAS era [7]. In the previous study, we identified rs1950834 as one of the 34 MDD risk SNPs that disrupt the binding of 15 TFs by integrating the ChIP-Seq and PWM data. Luciferase reporter assay showed higher luciferase activities of the G allele than the A allele of rs1950834 in HEK293T, SH-SY5Y, and SN-K-SH cells. However, no further investigation of the rs1950834 SNP was performed in that study [10]. Here, we elucidated that RAD21 and POLR2A were enriched in the DNA sequence flanking rs1950834, and targeted knockdown of these transcription factors reduced the expression of target genes *LRFN5*. In particular, we successfully established homozygous rs1950834-AA and rs1950834-GG genotypic SK-N-AS cells via single-base editing technology for the first time. We directly elucidated that the risk allele AA reduced *LRFN5* expression compared to the protective allele GG, even in the stress state of DEX intervention. Consequently, our results robustly support the notion that rs1950834 is a functional variant for MDD via regulating target gene expression.

Another important finding of this study is that *LRFN5* was selectively decreased in the NAc of MDD patients by meta-analysis of transcription data of MDD patients from the GEO database. Accordingly, LRFN5 expression was reduced in NAc neurons in CUMS-induced depression-like behavior mice, without the specificity of subregion and neuron subtype. Targeted knockdown of neuron-derived *Lrfn5* in NAc induced depression-like behaviors in mice and further aggravated the CUMS-induced phenotypes. On the contrary, *Lrfn5* overexpression in neurons can confer resistance to CUMS. The NAc is a component of the basal ganglia system and acts as a critical structure for reward and motivation-related behavior [68, 69]. Growing evidence supports that the NAc is a central brain region involved in affective circuits [70],

contributing to the pathophysiology and neuronal-circuit impairment of MDD [71–73]. Importantly, precise neuromodulation of NAc, such as deep brain stimulation, has been shown to play a significant antidepressant role [74, 75]. Taken together, the results indicated that the reduction of NAc neuron-derived *Lrfn5* leads to chronic stress-induced depression, which provides empirical evidence for precisely targeted antidepressants. On the other side, it should be noted that LRFN5 was also highly expressed in several brain regions, including amygdala, anterior cingulate cortex (BA24), caudate (basal ganglia), cerebellar hemisphere, cerebellum, cortex, frontal cortex (BA9), hippocampus, hypothalamus, putamen (basal ganglia), spinal cord (cervical c-1) and substantia nigra (Additional file 1: Fig. S3). Although this study is based on the findings of the human meta-analysis above, it first focuses on the NAs to reveal that the target gene is involved in chronic stress-induced depression in mice; we could not rule out the possibility that *LRFN5* contributes to MDD pathogenesis in other emotion-related brain regions. It should also be noted that examining multiple regions in meta-analysis increases the risk of false positives. Thereby, it is necessary for further detailed exploration.

This study also elucidated that the knockdown of *Lrfn5* in NAc neurons exacerbated CUMS-induced synaptic damage and depression-like behaviors in mice, while overexpression of *Lrfn*5 in NAc neurons reversed these phenotypes. LRFNs, also known as synaptic adhesion-like molecules (SALMs), are members of a family of synaptic adhesion molecules consisting of five known members: LRFN1-5 [16, 76, 77]. LRFN5 contains six leucine-rich repeats flanked by N-terminal and C-terminal cysteine-rich capping domains, an Ig domain, and a fibronectin III domain in the extracellular region, followed by a single transmembrane domain. LRFN5 was enriched in the synaptic fractions and could form complexes with PSD95 at excitatory synapses [18]. Knockdown of *Lrfn5* in cultured mouse hippocampal neurons inhibited the number of both excitatory and inhibitory synapses. Consistently, the frequencies and amplitudes of mEPSCs and mIPSCs were also reduced in *Lrfn5* knockdown neurons. Postsynaptic LRFN5 promotes synapse development and regulates AMPA-type glutamate receptor-mediated synaptic strength by trans-synaptically interacting with presynaptic leukocyte common antigen-related receptor protein tyrosine phosphatases [18, 20]. Importantly, we observed CUMS significantly reduced the frequency, but not amplitude, of mEPSCs in mice, indicating a decrease in AMPA receptor-mediated excitatory synaptic transmission. This reduction in mEPSCs frequency was ameliorated by *Lrfn5* overexpression. These findings consistently confirm that LRFN5 can be used as a molecular target to regulate synaptic function and MDD treatment, and provide evidence for NAc as a target area for neuromodulation.

Several limitations remain for this study. First, the discrepancy in the genomic location of rs1950834 in humans (14q21.1) and that of mouse *Lrfn5* (12qC1) complicactes the identification of the corresponding position of rs1950834 in mice. Consequently, the rs1950834 site-specific single-base edited mice could not be generated. Second, the absence of *Lrfn5* knockout or conditional knockout mice may have limited our ability to thoroughly elucidate the mechanisms underlying the protective role of *Lrfn5* on synaptic plasticity in depression. Third, it is necessary to note that *LRFN5* in other brain regions may also contribute to the pathogenesis of depressive disorder, together with NAc. For example, Levey et al. reported on the potential involvement of *LRFN5* in the frontal cortex in the pathogenesis of MDD [6, 15]. Therefore, further empirical investigations are required to validate these findings. In the future, we will also test whether LRFN5 is differentially expressed in neuron-derived exosomes of peripheral blood from MDD patients with a large sample size to establish a reliable diagnostic biomarker.

Conclusions

The study comprehensively elucidates the molecular regulatory mechanisms of MDD risk-associated variant rs1950834 at the single nucleotide level. The investigation has identified *LRFN5* as the target gene of rs1950834 and has suggested that NAc neuron-derived *LRFN5* was involved in depression by maintaining synapse-related functions. These findings provide valuable molecular and biological insights into the genetic regulatory mechanisms of MDD, offering a framework to elucidate functional variants at reported MDD risk loci. This study may broaden the boundaries of our understanding of MDD and provide new avenues for the development of novel therapeutic interventions.

Abbreviations

ACSF	Artificial cerebrospinal fluid
AMPA	α-Amino-3-hydroxy-5-methyl-4-isoxazole propionic acid
ChIP-seq	Chromatin immunoprecipitation-sequencing
CRISPR-Cas9	Clustered regularly interspaced short palindromic repeats (CRISPR)/CRISPR-associated protein 9 (Cas9)
CTCF	CCCTC-binding factor
CUMS	Chronic unpredictable mild stress
DAPI	4′,6-Diamidino-2-phenylindole
DEG	Differentially expressed gene
DEX	Dexamethasone
DNase	Deoxyribonuclease
DNase-seq	DNase I hypersensitive sites sequencing
DRD1	Dopamine receptor D1
DRD2	Dopamine receptor D2
EMSA	Electrophoretic mobility shift assay
ENCODE	Encyclopedia of DNA Elements
EPSC	Excitatory postsynaptic current
EZH2	Enhancer of zeste 2 polycomb repressive complex 2 subunits
FST	Forced swimming test
GEO	Gene Expression Omnibus
GFAP	Glial fibrillary acidic protein

GO	Gene ontology
GWAS	Genome-wide association study
Iba1	Ionized calcium-binding adaptor molecule 1
IF	Immunofluorescence
IPSC	Inhibitory postsynaptic current
KD	Knockdown
KEGG	Kyoto Encyclopedia of Genes and Genomes
L	Lateral
LD	Linkage disequilibrium
M	Medial
mEPSC	Miniature excitatory postsynaptic current
mIPSC	Miniature inhibitory postsynaptic current
MDD	Major depressive disorder
MSN	Medium spiny neuron
NAc	Nucleus accumbens
NeuN	Neuronal nuclei antigen
OE	Overexpression
OFT	Open-field test
POLR2 A	RNA polymerase II subunit A
PSD95	Postsynaptic density protein 95
PTPRD	Protein tyrosine phosphatase receptor type D
PWM	Position weight matrix
qPCR	Quantitative polymerase chain reaction
rAAV	Recombinant adeno-associated virus
RAD21	RAD21 cohesin complex component
SALM	Synaptic adhesion-like molecule
shRNA	Short hairpin RNA
siRNA	Small interfering RNA
SMARCA4	SWI/SNF related BAF chromatin remodeling complex subunit ATPase 4
SNAP25	Synaptosome associated protein 25
SNP	Single nucleotide polymorphism
SPT	Sucrose preference test
TF	Transcription factor
TST	Tail suspension test
WB	Western blot

Supplementary Information

The online version contains supplementary material available at https://doi.org/10.1186/s12916-025-04141-8.

Additional file 1. Fig.S1– rs1950834 allele frequencies in 1000 Genomes Project Phase 3 data. Fig. S2. Knockdown of RAD21 and POLR2A resulted in decreased expression of LRFN5. Fig. S3. rs1950834 showed a significant association with Lrfn5 expression in human brain regions. Fig. S4. RFN5 expression in different human tissues. Fig. S5. RFN5 expression in different human tissues. Fig. S6. LocusZoom plots for LRFN5 in the attention deficit and hyperactivity disorder, anorexia nervosa, anxiety disorder, autism spectrum disorder, bipolar disorder, and schizophrenia GWAS. Fig. S7. Meta-analysis of LRFN5 high expression of brain region in patients with MDD. Fig. S8. The EGFP tag expressed by the rAAV was co-labeled with neuronal marker NeuN, but not with markers of astrocytes (GFAP) or microglia (Iba1). Table S1. rs1950834 results in 101 brain regional volumes GWAS. Table S2. rs1950834 results in ENIGMA3 GWAS of cortical surface area and thickness. Table S3. rs1950834 results in the 33 K subjects brain image-derived phenotypes study. Table S4. PCR primers used for amplification of DNA sequence containing rs1950834 (for reporter gene assay). Table S5. Sequences of probes for EMSA. Table S6. ChIP-qPCR primers. Table S7. sgRNA primers used to knockout DNA fragments containing rs1950834. Table S8. PCR primers for qPCR. Table S9. The gRNA and ssDNA used to single-base editing of rs1950834. Table S10. Sequences of shRNAs used to knockdown RAD21 and POLR2A. Table S11. Reagents and resources. Table S12. PCR primers for detection of mycoplasma contamination. Table S13. Sequences of shRNAs used to knockdown LRFN5. Graph Abstract.

Additional file 2. The original, uncropped gels/blots

Additional file 3. The ARRIVE guidelines

Acknowledgements
Not applicable.

Authors' contributions
Z. Z., X. L., and Y. K. were responsible for the overall design and guidance of the experiment, and Z. Z. and Y. K. were responsible for the writing and revision of draft articles. D. L., Q. B., and T. Z. completed the experimental work, and D. L. partly participated in the draft preparation in the beginning. Y. L. guided graduate students X. C., X. D., and J. W. through the in vitro experiments and bioinformatics analysis, respectively, and Y. L. participated in draft writing, charting, and revision. Y. S. helps D. L. to build animal models. Under the guidance of Y. Z., T. Z., and S. J. collaborated to complete the model animal electrophysiology-related experiments and documentation. A. Z. generated the figures and tables under the guidance of Profs Z. Z., Y. K., and Y. L. All authors read and approved the manuscript.

Funding
This study was supported by China Science and Technology Innovation 2030—Major Project (2022ZD0211701, 2022ZD0211704 and 2021ZD0200700), National Natural Science Foundation of China (82471552, 82130042, 82371532, U2102205 and 82301690), Shenzhen Science and Technology Serial Funds (GJHZ20210705141400002, KCXFZ20211020164543006, JCYJ20220818101615033, ZDSYS20220606100606014, and KQTD20221101093608028), Postdoctoral Fellowship Program of CPSF (GZB20230136), and Open Program of Henan Key Laboratory of Biological Psychiatry (ZDSYS2022001).

Data availability
The data that support the findings of this study are available in ENCODE, PsychENCODE, The data that support the findings of this study are available from publicly accessible resources, including the Ensemble, https://www.ensembl.org/index.html; PsychENCODE, UCSC genome browser, https://genome.ucsc.edu/; SZDB, http://www.szdb.org.cn/index.html, RegulomeDB, https://regulomedb.org/regulome-search/; BrainSpan atlas, http://www.brainspan.org/; 3D Interaction Viewer and database (3DIV), https://kobic.kr/3divv1/; UCSC cell Browser https://cells.ucsc.edu/; the comprehensive human Super-Enhancer database (SEdb), and Human Protein Atlas, https://www.proteinatlas.org/. The datasets used and/or analysed during the current study are available from the corresponding author on reasonable request. The data of high-throughput RNA sequencing performed in this study have been deposited in the GEO database (reference number: GSE296333).

Declarations

Ethics approval and consent to participate
The use of animals in this experiment was approved by the Animal Experimentation Ethics Committee of Southeast University (20220104003 and 20221014001).

Consent for publication
Not applicable.

Competing interests
The authors declare no competing interests.

Author details
[1]Department of Neurology in Affiliated Zhongda Hospital and Jiangsu Provincial Medical Key Discipline, School of Medicine, Research Institute of Neuropsychiatry, Key Laboratory of Developmental Genes and Human Disease of the Ministry of Education, Southeast University, Nanjing 210096, China. [2]Shenzhen Key Laboratory of Precision Diagnosis and Treatment of Depression, Department of Mental Health and Public Health in Faculty of Life and Health Sciences of Shenzhen University of Advanced Technology, The Brain Cognition and Brain Disease Institute of Shenzhen Institute of Advanced Technology, Chinese Academy of Sciences, Shenzhen 518055, China. [3]The Second Affiliated Hospital of Kunming Medical University, Kunming 650223, China. [4]Department of Human Anatomy, School of Basic Medical Sciences, Zhengzhou University, Zhengzhou, Henan 450001, China. [5]Key Laboratory of Optical Technology and Instrument for Medicine, Ministry of Education; School of Optical-Electrical Computer Engineering, University of Shanghai for Science and Technology, Shanghai 200093, China. [6]Shenzhen

Key Laboratory of Drug Addiction, Shenzhen Neher Neural Plasticity Laboratory, the Brain Cognition and Brain Disease Institute, Shenzhen Institute of Advanced Technology, Chinese Academy of Sciences, Shenzhen 518055, China. [7]Department of Biochemistry and Molecular Biology, School of Medicine, Southeast University, Nanjing, Jiangsu 210009, China.

Received: 8 January 2025 Accepted: 15 May 2025
Published online: 30 May 2025

References

1. Sullivan PF, Daly MJ, O'Donovan M. Genetic architectures of psychiatric disorders: the emerging picture and its implications. Nat Rev Genet. 2012;13:537–51.
2. CONVERGE consortium. Sparse whole-genome sequencing identifies two loci for major depressive disorder. Nature. 2015;523:588–91.
3. Wray NR, Ripke S, Mattheisen M, Trzaskowski M, Byrne EM, Abdellaoui A, et al. Genome-wide association analyses identify 44 risk variants and refine the genetic architecture of major depression. Nat Genet. 2018;50:668–81.
4. Howard DM, Adams MJ, Clarke T-K, Hafferty JD, Gibson J, Shirali M, et al. Genome-wide meta-analysis of depression identifies 102 independent variants and highlights the importance of the prefrontal brain regions. Nat Neurosci. 2019;22:343–52.
5. Als TD, Kurki MI, Grove J, Voloudakis G, Therrien K, Tasanko E, et al. Depression pathophysiology, risk prediction of recurrence and comorbid psychiatric disorders using genome-wide analyses. Nat Med. 2023;29:1832–44.
6. Meng X, Navoly G, Giannakopoulou O, Levey DF, Koller D, Pathak GA, et al. Multi-ancestry genome-wide association study of major depression aids locus discovery, fine mapping, gene prioritization and causal inference. Nat Genet. 2024;56:222–33.
7. Gallagher MD, Chen-Plotkin AS. The post-GWAS era: from association to function. Am J Hum Genet. 2018;102:717–30.
8. Xu K, Zheng P, Zhao S, Wang J, Feng J, Ren Y, et al. LRFN5 and OLFM4 as novel potential biomarkers for major depressive disorder: a pilot study. Transl Psychiatry. 2023;13:188.
9. Dall'Aglio L, Lewis CM, Pain O. Delineating the genetic component of gene expression in major depression. Biol Psychiatry. 2021;89:627–36.
10. Li S, Li Y, Li X, Liu J, Huo Y, Wang J, et al. Regulatory mechanisms of major depressive disorder risk variants. Mol Psychiatry. 2020;25:1926–45.
11. Howard DM, Adams MJ, Shirali M, Clarke T-K, Marioni RE, Davies G, et al. Genome-wide association study of depression phenotypes in UK Biobank identifies variants in excitatory synaptic pathways. Nat Commun. 2018;9:1470.
12. 1000 Genomes Project Consortium, Abecasis GR, Altshuler D, Auton A, Brooks LD, Durbin RM, et al. A map of human genome variation from population-scale sequencing. Nature. 2010;467:1061–73.
13. Li H-J, Qu N, Hui L, Cai X, Zhang C-Y, Zhong B-L, et al. Further confirmation of netrin 1 receptor (DCC) as a depression risk gene via integrations of multi-omics data. Transl Psychiatry. 2020;10:98.
14. Zheng H, Sun J, Pang T, Liu J, Lu L, Chang S. Identify novel, shared and disorder-specific genetic architecture of major depressive disorder, insomnia and chronic pain. J Psychiatr Res. 2022;155:511–7.
15. Levey DF, Stein MB, Wendt FR, Pathak GA, Zhou H, Aslan M, et al. Bi-ancestral depression GWAS in the Million Veteran Program and meta-analysis in >1.2 million individuals highlight new therapeutic directions. Nat Neurosci. 2021;24:954–63.
16. Morimura N, Inoue T, Katayama K, Aruga J. Comparative analysis of structure, expression and PSD95-binding capacity of Lrfn, a novel family of neuronal transmembrane proteins. Gene. 2006;380:72–83.
17. Homma S, Shimada T, Hikake T, Yaginuma H. Expression pattern of LRR and Ig domain-containing protein (LRRIG protein) in the early mouse embryo. Gene Expr Patterns. 2009;9:1–26.
18. Mah W, Ko J, Nam J, Han K, Chung WS, Kim E. Selected SALM (synaptic adhesion-like molecule) family proteins regulate synapse formation. J Neurosci. 2010;30:5559–68.
19. Nam J, Mah W, Kim E. The SALM/Lrfn family of leucine-rich repeat-containing cell adhesion molecules. Semin Cell Dev Biol. 2011;22:492–8.
20. Choi Y, Nam J, Whitcomb DJ, Song YS, Kim D, Jeon S, et al. SALM5 trans-synaptically interacts with LAR-RPTPs in a splicing-dependent manner to regulate synapse development. Sci Rep. 2016;6:26676.
21. Li D, Hsu S, Purushotham D, Sears RL, Wang T. WashU Epigenome Browser update 2019. Nucleic Acids Res. 2019;47:W158–65.
22. ENCODE Project Consortium. An integrated encyclopedia of DNA elements in the human genome. Nature. 2012;489:57–74.
23. Davis CA, Hitz BC, Sloan CA, Chan ET, Davidson JM, Gabdank I, et al. The Encyclopedia of DNA elements (ENCODE): data portal update. Nucleic Acids Res. 2018;46:D794-801.
24. Wagih O. ggseqlogo: a versatile R package for drawing sequence logos. Bioinformatics. 2017;33:3645–7.
25. Merkenschlager M, Wang Y, Weiss F. Activity-induced gene expression and long-range enhancer-promoter contacts in cohesin-deficient neurons with BDNF. GEO http://identifiers.org/geo:GSE172425 (2022)
26. Maslon MM, Braunschweig U, Aitken S, Mann AR, Kilanowski F, Hunter CJ, et al. Slow transcriptional elongation causes embryonic lethality and perturbs kinetic coupling of long neural genes [RNA-seq]. https://www.ncbi.nlm.nih.gov/geo/query/acc.cgi?acc=GSE125413 (2019)
27. Pantazatos SP, Arango V, Mann JJ. Whole-transcriptome brain expression and exon-usage profiling in major depression and suicide. https://www.ncbi.nlm.nih.gov/geo/query/acc.cgi?acc=GSE101521 (2017)
28. Labonte B, Engmann O, Purushothaman I, Ménard C, Wang J, Tan C, at al. Sex-specific transcriptional signatures in human depression. https://www.ncbi.nlm.nih.gov/geo/query/acc.cgi?acc=GSE102556 (2017)
29. Vadodaria KC, Gage FH. Serotonin-induced hyperactivity in SSRI-resistant major depressive disorder patient-derived neurons. https://www.ncbi.nlm.nih.gov/geo/query/acc.cgi?acc=GSE125664 (2019)
30. Vadodaria KC, Gage FH. Altered serotonergic circuitry in SSRI-resistant major depressive disorder patient-derived neurons. https://www.ncbi.nlm.nih.gov/geo/query/acc.cgi?acc=GSE126512 (2022)
31. Dmitrzak-Weglarz M, Banach E, Bilska K, Narozna B, Szczepankiewicz A, Reszka E, et al. Molecular regulation of melatonin biosynthesis pathway in unipolar and bipolar depression. https://www.ncbi.nlm.nih.gov/geo/query/acc.cgi?acc=GSE169459 (2021)
32. Oh H, Newton DF, Sibille EL. Cell-specific transcriptomic analysis of CRH+ cells identifies unique cellular responses to chronic stress. https://www.ncbi.nlm.nih.gov/geo/query/acc.cgi?acc=GSE193417 (2022)
33. Yi Z, Li Z. Expression data from peripheral blood lymphocytes of major depression, subsyndromal symptomatic depression, and healthy controls. https://www.ncbi.nlm.nih.gov/geo/query/acc.cgi?acc=GSE32280 (2012)
34. Bergon A, Belzeaux R, Loriod B, Jeanjean V, Verrier L, Ibrahim E. Transcription profiling of major depression peripheral blood mononuclear cells (PBMCs) at clinical remission compared to severe acute state. https://www.ncbi.nlm.nih.gov/geo/query/acc.cgi?acc=GSE38206 (2012)
35. Frank B, Savitz J, Bebak M, Marino JH, Teague TK, Drevets WC. Differential gene expression in patients with mood disorders. https://www.ncbi.nlm.nih.gov/geo/query/acc.cgi?acc=GSE39653 (2012)
36. Sibille E. Molecular evidence for a dimensional basis of depression. https://www.ncbi.nlm.nih.gov/geo/query/acc.cgi?acc=GSE44593 (2016).
37. Lanz TA. Microarray profiling of PFC, HPC and STR from subjects with schizophrenia, bipolar, MDD or control. https://www.ncbi.nlm.nih.gov/geo/query/acc.cgi?acc=GSE53987 (2014).
38. Sibille E. Expression data from human brain anterior cingulate cortex - including control samples and samples with major depression disorders (20 samples MD2_ACC). https://www.ncbi.nlm.nih.gov/geo/query/acc.cgi?acc=GSE54562 (2014)
39. Sibille E. Expression data from human brain anterior cingulate cortex - including control samples and samples with major depression disorders (50 samples MD3_ACC). https://www.ncbi.nlm.nih.gov/geo/query/acc.cgi?acc=GSE54563 (2014)
40. Sibille E. Expression data from human brain amygdala - including control samples and samples with major depression disorders (42 samples MD3_AMY). https://www.ncbi.nlm.nih.gov/geo/query/acc.cgi?acc=GSE54564 (2014)
41. Sibille E. Expression data from human brain anterior cingulate cortex - including control samples and samples with major depression disorders (32 samples MD1_ACC). https://www.ncbi.nlm.nih.gov/geo/query/acc.cgi?acc=GSE54565 (2014)

42. Sibille E. Expression data from human brain amygdala - including control samples and samples with major depression disorders (28 samples MD1_AMY). https://www.ncbi.nlm.nih.gov/geo/query/acc.cgi?acc=GSE54566 (2014)
43. Sibille E. Expression data from human brain dorsolateral prefrontal cortex - including control samples and samples with major depression disorders (28 samples BA9_M). https://www.ncbi.nlm.nih.gov/geo/query/acc.cgi?acc=GSE54567 (2014)
44. Sibille E. Expression data from human brain dorsolateral prefrontal cortex - including control samples and samples with major depression disorders (30 samples BA9_F). https://www.ncbi.nlm.nih.gov/geo/query/acc.cgi?acc=GSE54568 (2014)
45. Sibille E. Expression data from human brain anterior cingulate cortex - including control samples and samples with major depression disorders (26 samples BA25_F). https://www.ncbi.nlm.nih.gov/geo/query/acc.cgi?acc=GSE54571 (2014)
46. Sibille E. Expression data from human brain anterior cingulate cortex - including control samples and samples with major depression disorders (24 samples BA25_M). https://www.ncbi.nlm.nih.gov/geo/query/acc.cgi?acc=GSE54572 (2014)
47. Miyata S, Okano Y, Sakurai N, Takahashi K, Narita K, Fukuda M, Mikuni M. Blood transcriptomic markers in patients with late-onset major depressive disorder. https://www.ncbi.nlm.nih.gov/geo/query/acc.cgi?acc=GSE76826 (2016).
48. Bowling KM, Ramaker RC, Lasseigne BN, Cooper SJ, Myers RM. RNA-sequencing of human post-mortem brain tissues. https://www.ncbi.nlm.nih.gov/geo/query/acc.cgi?acc=GSE80655 (2017)
49. Kelly FM, Leday GG, Vértes PE, Richardson S, Greene JR, Regan T, et al. https://www.ncbi.nlm.nih.gov/geo/query/acc.cgi?acc=GSE98793 (2017)
50. Snijders GJLJ, Sneeboer MAM, Fernández-Andreu A, Udine E, Psychiatric donor program of the Netherlands Brain Bank (NBB-Psy), Boks MP, et al. Distinct non-inflammatory signature of microglia in post-mortem brain tissue of patients with major depressive disorder. Mol Psychiatry. 2021;26:3336–49.
51. Lu Q, Wu F, Jiao J, Xue L, Song R, Shi Y, et al. Selective activation of ABCA1/ApoA1 signaling in the V1 by magnetoelectric stimulation ameliorates depression via regulation of synaptic plasticity. iScience. 2022;25:104201.
52. Kong Y, Zhang X, Li L, Zhao T, Huang Z, Zhang A, et al. Microglia-derived vitamin D binding protein mediates synaptic damage and induces depression by binding to the neuronal receptor megalin. Adv Sci (Weinh). 2024;12:e2410273.
53. Noh K, Cho W-H, Lee BH, Kim DW, Kim YS, Park K, et al. Cortical astrocytes modulate dominance behavior in male mice by regulating synaptic excitatory and inhibitory balance. Nat Neurosci. 2023;26:1541–54.
54. Zhu Y, Wienecke CFR, Nachtrab G, Chen X. A thalamic input to the nucleus accumbens mediates opiate dependence. Nature. 2016;530:219–22.
55. Miller DE, Patel ZH, Lu X, Lynch AT, Weirauch MT, Kottyan LC. Screening for functional non-coding genetic variants using electrophoretic mobility shift assay (EMSA) and DNA-affinity precipitation assay (DAPA). J Vis Exp. 2016;114:54093.
56. Hellman LM, Fried MG. Electrophoretic mobility shift assay (EMSA) for detecting protein-nucleic acid interactions. Nat Protoc. 2007;2:1849–61.
57. Walker RL, Ramaswami G, Hartl C, Mancuso N, Gandal MJ, de la Torre-Ubieta L, et al. Genetic control of expression and splicing in developing human brain informs disease mechanisms. Cell. 2019;179:750-771.e22.
58. Calderon L, Weiss FD, Beagan JA, Oliveira MS, Georgieva R, Wang Y-F, et al. Cohesin-dependence of neuronal gene expression relates to chromatin loop length. Elife. 2022;11: e76539.
59. Maslon MM, Braunschweig U, Aitken S, Mann AR, Kilanowski F, Hunter CJ, et al. A slow transcription rate causes embryonic lethality and perturbs kinetic coupling of neuronal genes. EMBO J. 2019;38: e101244.
60. Li W, Chen R, Feng L, Dang X, Liu J, Chen T, et al. Genome-wide meta-analysis, functional genomics and integrative analyses implicate new risk genes and therapeutic targets for anxiety disorders. Nat Hum Behav. 2024;8:361–79.
61. Dang X, Teng Z, Yang Y, Li W, Liu J, Hui L, et al. Gene-level analysis reveals the genetic aetiology and therapeutic targets of schizophrenia. Nat Hum Behav. 2025. https://doi.org/10.1038/s41562-024-02091-4.
62. Demontis D, Walters RK, Martin J, Mattheisen M, Als TD, Agerbo E, et al. Discovery of the first genome-wide significant risk loci for attention deficit/hyperactivity disorder. Nat Genet. 2019;51:63–75.
63. Watson HJ, Yilmaz Z, Thornton LM, Hübel C, Coleman JRI, Gaspar HA, et al. Genome-wide association study identifies eight risk loci and implicates metabo-psychiatric origins for anorexia nervosa. Nat Genet. 2019;51:1207–14.
64. Grove J, Ripke S, Als TD, Mattheisen M, Walters RK, Won H, et al. Identification of common genetic risk variants for autism spectrum disorder. Nat Genet. 2019;51:431–44.
65. Mullins N, Forstner AJ, O'Connell KS, Coombes B, Coleman JRI, Qiao Z, et al. Genome-wide association study of more than 40,000 bipolar disorder cases provides new insights into the underlying biology. Nat Genet. 2021;53:817–29.
66. Floresco SB. The nucleus accumbens: an interface between cognition, emotion, and action. Annu Rev Psychol. 2015;66:25–52.
67. Stratton HJ, Khanna R. Sculpting dendritic spines during initiation and maintenance of neuropathic pain. J Neurosci. 2020;40:7578–89.
68. Kopec AM, Smith CJ, Ayre NR, Sweat SC, Bilbo SD. Microglial dopamine receptor elimination defines sex-specific nucleus accumbens development and social behavior in adolescent rats. Nat Commun. 2018;9:3769.
69. Zhao J, Ying L, Liu Y, Liu N, Tu G, Zhu M, et al. Different roles of Rac1 in the acquisition and extinction of methamphetamine-associated contextual memory in the nucleus accumbens. Theranostics. 2019;9:7051–71.
70. Tarazi FI, Tomasini EC, Baldessarini RJ. Postnatal development of dopamine D1-like receptors in rat cortical and striatolimbic brain regions: an autoradiographic study. Dev Neurosci. 1999;21:43–9.
71. Nardou R, Sawyer E, Song YJ, Wilkinson M, Padovan-Hernandez Y, de Deus JL, et al. Psychedelics reopen the social reward learning critical period. Nature. 2023;618:790–8.
72. Birnie MT, Short AK, de Carvalho GB, Taniguchi L, Gunn BG, Pham AL, et al. Stress-induced plasticity of a CRH/GABA projection disrupts reward behaviors in mice. Nat Commun. 2023;14:1088.
73. Chen G, Lai S, Bao G, Ke J, Meng X, Lu S, et al. Distinct reward processing by subregions of the nucleus accumbens. Cell Rep. 2023;42: 112069.
74. Zhu Y, Wang K, Ma T, Ji Y, Lou Y, Fu X, et al. Nucleus accumbens D1/D2 circuits control opioid withdrawal symptoms in mice. J Clin Invest. 2023;133: e163266.
75. Dandekar MP, Fenoy AJ, Carvalho AF, Soares JC, Quevedo J. Deep brain stimulation for treatment-resistant depression: an integrative review of preclinical and clinical findings and translational implications. Mol Psychiatry. 2018;23:1094–112.
76. Ko J, Kim S, Chung HS, Kim K, Han K, Kim H, et al. SALM synaptic cell adhesion-like molecules regulate the differentiation of excitatory synapses. Neuron. 2006;50:233–45.
77. Wang C-Y, Chang K, Petralia RS, Wang Y-X, Seabold GK, Wenthold RJ. A novel family of adhesion-like molecules that interacts with the NMDA receptor. J Neurosci. 2006;26:2174–83.

Publisher's Note